CORE
Metadata, citation and similar papers at core.ac.uk
Provided by DCU Online Research Access Service

Photoluminescence and Excitation Studies of Semiconductors

A thesis for the degree of
MASTER OF SCIENCE

Presented to
DUBLIN CITY UNIVERSITY

by

DERMOT GORMAN B Sc

Research Supervisor
PROF MARTIN O HENRY
School of Physical Sciences
Dublin City University

September 2001

Declaration

I hereby certify that this material, which I now submit for assessment on the programme of study leading to the award of Master of Science is entirely my own work and has not been taken from the work of others save and to the extent that such work has been cited and acknowledged within the text of my work.

Signed: Dermot Gorman ID No.: 95306161

Dermot Gorman

Date: 29/09/01

Acknowledgements

I would like to extend my sincerest gratitude to Prof Martin Henry for allowing me the opportunity to pursue this research and for sharing with me his vast knowledge of semiconductor physics His support and commitment to this study was greatly appreciated

I would especially like to thank Dr Enda McGlynn for his support, guidance and invaluable advice throughout this study

To my parents, sisters and brother for their support and to my sister, Catherine, for proof reading this thesis

Abstract

A photoluminescence (PL) study of Be and Au ion-implanted GaN is presented GaN samples were implanted and selectively annealed prior to excitation by a HeCd laser The resulting luminescence was dispersed by a grating spectrometer and detected using a photomultiplier tube Be is proposed to form a shallow acceptor in GaN and is thus critical to device development and performance From analysis of the PL spectra, a shallow level appears consistently following an annealing procedure

It has been observed that Au impurities in Si introduce centres near the middle of the bandgap which act as very effective lifetime killers A PL study of the effect of Au impurities in GaN is presented A series of bands occur in the region 1 5eV to 2 4eV with peaks at 1 7eV and 2 3eV

A parallel aspect of the work involved the development of a photoluminescence excitation (PLE) spectroscopy system with the ultimate aim of investigating impurity centres in doped GaN The PLE system consisted of a tunable laser source, existing photoluminescence equipment and a computer control / acquisition system PLE is used to investigate the below bandgap optical characteristics of emission bands and levels Preliminary results using this equipment on well characterised ruby samples are presented along with a study of Be and Au defects in GaN

Contents

1 Introduction **7**

2 Semiconductor Physics - Theory **8**

2 1 Introduction 8

2 2 Band Theory of Semiconductors 8

2 3 Recombination Processes in Semiconductors 10

3 Gallium Nitride **14**

3 1 Introduction 14

3 2 Material Characteristics 14

3 3 Growth Techniques 14

3 4 N and P Type Dopants in GaN 16

4 Photoluminescence System **20**

4 1 Introduction 20

4 2 Photoluminescence Theory 20

4 3 Experimental System 21

4 3 1 Laser Excitation Source 21

4 3 2 Spectrometer 22

4 3 3 Photomultiplier Detector 23

4 3 4 Continuous Flow Cryostat 25

4 4 System Calibration 25

5 Photoluminescence Results **29**

5 1 Introduction 29

5 2 Sample Preparation 29

5 3 Be Impanted GaN 31

5 3 1 Be Implanted GaN at $1 \times 10^{12}\text{cm}^{-2}$ 34

5 3 2 Be Implanted GaN at $1 \times 10^{13}\text{cm}^{-2}$ 37

5 3 3 Be Implanted GaN at $1 \times 10^{14}\text{cm}^{-2}$ 39

5 4 Discussion 41

5 5 Au Implanted GaN 45
5 6 Discussion 47

6 PLE System Development 50
6 1 Introduction 50
6 2 Photoluminescence Excitation Theory 50
6 3 Experimental System 51
6 3 1 OPO Excitation Source 52
6 3 2 System Development 54
6 4 Conclusion 61

7 PLE Results 63
7 1 Introduction 63
7 2 Ruby Results 63
7 3 Au Implanted GaN 66
7 4 Be implanted GaN 69
7 5 Conclusions and suggestions for future work 73

A Grating Efficiency equations 75

B LabView Source Code for PLE System 76

1 Introduction

Semiconductor materials have been at the centre of condensed matter physics research for many decades, and this situation has not changed up to the present day As a multi-billion dollar semiconductor industry hungers for better performance of their devices, physicists and material scientists work diligently to satisfy the demand New materials rise to the spotlight while the properties of old ones become better known The position of silicon as the major semiconductor material has not yet been shaken However, the demand for new materials created and engineered for specific applications has led to the rise of compound semiconductors, an example of which is the III-V material Gallium Nitride (GaN) These III-V materials are being developed and actively researched by both academic and commercial sectors due to their physical properties and potential device applications GaN holds much interest for short wavelength optical devices, high power electronics and high temperature electronics The main attraction of GaN is its large direct bandgap suitable for short wavelength LED's and laser diodes GaN has been commercialised in this area and such devices are operational in the blue and UV region of the spectrum Significant applications are born from the short wavelength of these devices, for example optical data storage (DVD) and high resolution laser printing Other example applications include projection displays, full colour outdoor TV displays and traffic signals

Continuous research and development is carried out on the material properties used to create these optoelectronic devices The aim of researchers is to engineer devices with specific and reproducible performance characteristics The study presented here investigates the effect of introducing impurity elements into the bandgap of GaN Samples are characterised using photoluminescence and photoluminescence excitation spectroscopy to identify the optical processes operating within the bandgap

2 Semiconductor Physics - Theory

2.1 Introduction

In order to analyse photoluminescence (PL) and photoluminescence excitation (PLE) spectra and to understand the operation of semiconductor devices, an appreciation of the solid state physics involved in these materials is required The relevant concepts behind band structure of semiconductors are reviewed here

2.2 Band Theory of Semiconductors

An understanding of the band theory of semiconductors is achieved by solving the Schrodinger equation for an electron in a three dimensional box This is treated at a simple level by Rudden *et al* [1] This model assumes a free electron and the solution gives a series of discrete energy levels Figure 1(a) represents the continuous E versus k curve for a free electron However, the Kronig-Penney model predicts that discontinuities will occur on this parabolic E versus k curve when $k = \frac{n\pi}{a}$ As isolated atoms are brought together to form an ideal crystalline solid, important changes occur in the electron energy levels due to the overlap of electron wavefunctions They split into energy levels belonging to the collection of atoms as a whole These discrete levels spread out into a range of sublevels which are so close together that they are termed bands and are separated by forbidden energy gaps (figure 1(b)) In figure 1(b) the E versus k curve is redrawn using the reduced zone scheme by translating all segments to lie within $\pm\frac{\pi}{a}$ k values This representation is much more complex in real solids where the E versus k curves depend on the direction of the electron wave vector with respect to the crystallographic axes

The nature of a given solid is determined by the size of the energy gap, E_g, and extent to which these bands are occupied, among other factors This energy gap or 'forbidden' bandgap region lies between the minimum of the

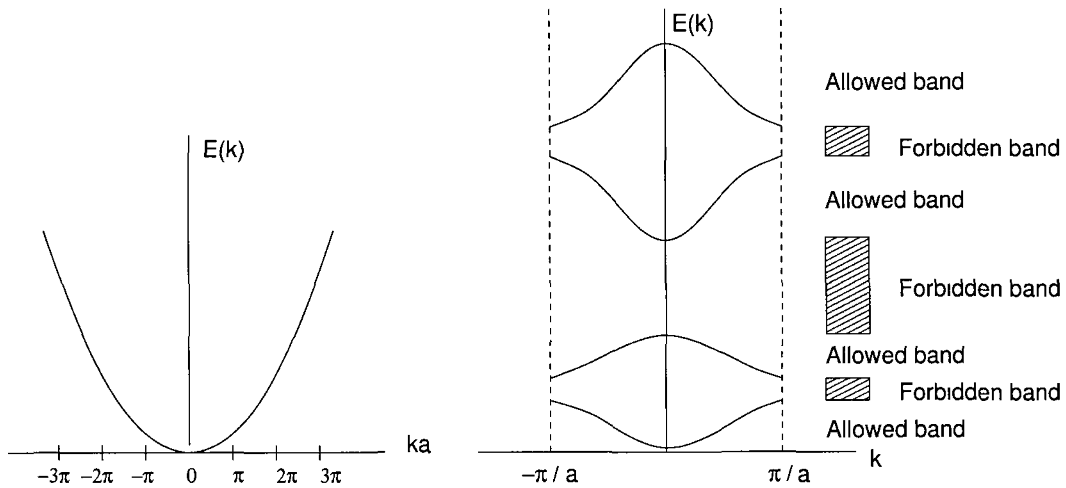

Figure 1 (a) Energy versus wavevector k for a free electron Kronnig-Penney model predicts discontinuities at $\pm n\pi/a$ (b) Reduced zone representation of the E versus k curve where all segments are translated to lie in the region $-\pi/a < k < \pi/a$

conduction band and the maximum of the valence band The size of this gap determines whether the material is an insulator, conductor or a semiconductor With a large gap, thermal energies are too small to promote electrons from the lower valence band to the conduction band Such a material has very few free carriers at room temperature and is said to be insulating Semiconductors become more conducting with increasing temperature or with illumination by high energy photons or radioactive particles With a smaller gap, thermal energy can excite electrons to the conduction band, the numbers depending on the temperature Semiconductors behave like a poor metal at high temperatures and insulators at low temperatures The value of gap energy separating semiconductors from insulators is arbitrary, but is often taken as 3eV [2], an energy which thermal electrons obtain at a temperature of 37,000K For comparison, the gap energy of elemental Si is 1 12eV [3] and that of the wide band gap material GaN is 3 503eV [4] (at low temperatures) This energy gap represents a threshold energy for light absorption if the semiconductor sample is perfect Light absorption increases

at energies above the bandgap, the rate being very abrupt for direct bandgap semiconductors like GaN [5]

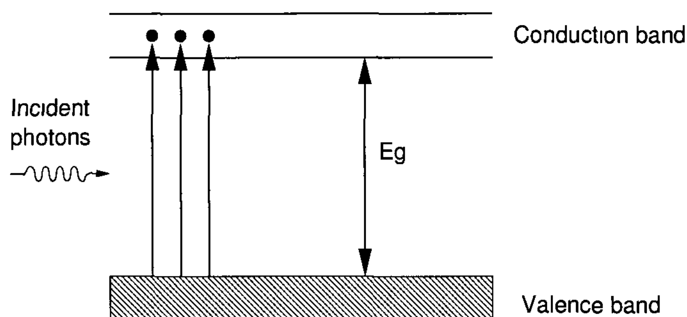

Figure 2 Photoexcitation of electrons from the valence band to the conduction band due to the absorption of photons of energy $hv \geq E_g$

For the purposes of optical characterisation of semiconductors the forbidden bandgap region is of primary interest From the point of view of optoelectronics an electron can be promoted from the valence band to the conduction band if it absorbs a photon with energy at least equal to the gap value (see figure 2) In the case of GaN, if we excite the sample with the 325nm (3 825eV) line of a HeCd laser, the sample is flooded with photons of energy large enough to excite electrons above the 3 5eV energy gap This optical absorption process creates carriers in excess of the thermal equilibrium values which will ultimately die out through recombination

2.3 Recombination Processes in Semiconductors

Typical recombination processes which can occur in semiconductors are free excitons (F_x), band-to-band (e-h), carrier to localised impurity states (e-A, D-h) and carriers bound to other impurities (D-A), these are illustrated in figure 3 (where e and h are the electron and hole carriers respectively and D and A represent the donor and acceptor impurity levels)

The free exciton is a level similarly placed to that of a donor level which can appear in intrinsic materials These arise because the Coulombic attraction of an electron to a hole can result in the two being bound together

forming a quasi particle called an exciton, denoted F_x. This can be visualised as a Bohr-like state where an electron and hole circle around their common center of gravity at relatively large distances [6]. Exciton states situated just below the conduction band are weakly bound with a binding energy of

$$E_x \simeq 13.6 \frac{m_r^*}{m} \left(\frac{1}{\epsilon_r}\right)^2 \tag{1}$$

Excitons may move through a crystalline lattice and provide an important means of transferring energy from one point to another. The recombination energy of a free exciton (F_x) in a direct bandgap semiconductor (like GaN) is given by

$$hv = E_g - E_x \tag{2}$$

where E_x is the exciton binding energy. In a material with impurities, the free exciton can be trapped at one of these impurities and become bound there, resulting in the label bound-exciton (BE) with a recombination energy of

$$hv = E_g - E_x - E_T \tag{3}$$

where E_T is the energy of the trapped exciton relative to the free exciton. Because exciton binding energies in most materials are quite low (50-100meV in Si), excitons can only be seen in pure samples of these materials at low temperatures. In less pure materials or at higher temperatures the exciton is dissociated into separate particles which can recombine in a band-to-band transition.

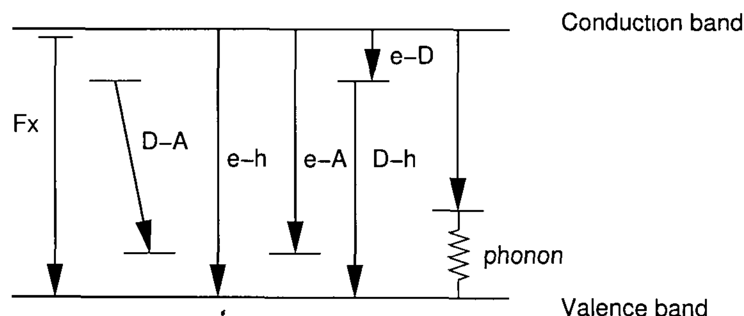

Figure 3 Different possible recombination paths available [7]

The presence of lattice defects and doping with n and p type impurity elements can result in the formation of new energy states within the forbidden gap Carriers can become trapped at these impurity states and the resulting recombination can dominate the luminescence spectra Controlled doping with impurity elements can create levels situated just below the conduction band (donor level) or above the valence band (acceptor level) A donor level provides an excess of electrons which are easily excited to the conduction band thus increasing the free electron concentration and hence the conductivity of the material An acceptor level traps electrons excited from the valence band leaving behind electron vacancy termed a 'hole' These holes are now the majority carriers and the dominant form of conduction

In addition to radiative processes, non-radiative processes can also contribute significantly to annihilation of excess electrons and holes in the form of phonons These processes in many cases result in unacceptably low efficiencies rendering the devices or materials technologically and commercially insignificant

References

[1] Rudden & Wilson, Elements of Solid State Physics, (2nd Edition Wiley New York, 1993), pp 121-125

[2] Perkowitz S , Optical Characterization of Semiconductors, (Academic Press London, 1993), pp 19

[3] Parker G , Introductory semiconductor device physics, (Prentice Hall, 1994), pp 13

[4] Orton & Foxon, Group III nitride semiconductors for short wavelength light-emitting devices, Rep Prog Phys 61, (1998), pp 22

[5] Gil B , Beyond silicon the rise of compound semiconductors, O'Donnell Kevin, Group III Nitride semiconductor compounds Ch 1, (Oxford Science Publications, 1998)

[6] Wilson & Hawkes, Optoelectronics - An Introduction, (Prentice Hall Int series of optoelectronics, 1989), pp 147

[7] Basu P K , Theory of Optical Processes in Semiconductors, (Oxford University Press, 1997), pp 205-206

3 Gallium Nitride

3.1 Introduction

The wide bandgap and high luminescence efficiency of III-V nitride semiconductors make them superior materials for optoelectronic devices operating in the UV to visible spectral region The properties of GaN relevant to this work are reviewed in this chapter

3.2 Material Characteristics

GaN is a direct bandgap semiconductor with an optical bandgap energy of 3 503eV [1] (at 10K) GaN can crystallise in both the hexagonal wurzite structure and the cubic zinc blende form, the thermodynamically stable structure being the wurzite structure [2] The electronic band structure is strongly influenced by the crystal phase Both crystalline structures have a band structure showing a direct optical transition between the conduction band and the valence band at the Γ-point (k=0) The calculated electronic band structure for the wurzite phase is shown in figure 4 The bandgap energy of GaN can be fitted to the Varshni formula [3] (fitted by Monemar) with an experimental uncertainty of 2meV

$$E_g = 3\ 503 + (5\ 08 \times 10^{-4} T^2)/(T - 996) eV \qquad (4)$$

3.3 Growth Techniques

Group III-V nitride compounds like GaN do not exist in nature and must be artificially synthesised using a variety of possible growth methods Such methods include Metal Organic Chemical Vapour Deposition (MOCVD), Molecular Beam Epitaxy (MBE), Hydride Vapour Phase Epitaxy (HVPE) and more recently, Pulsed Laser Deposition (PLD) [4] The quality of GaN films is typically judged using three different criteria, namely [5]

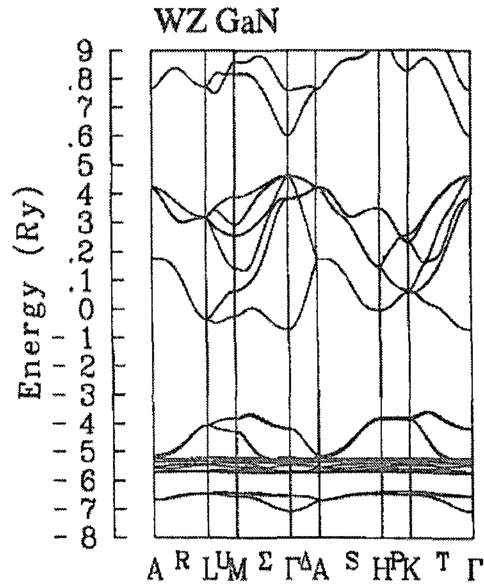

Figure 4 Calculated electronic band structure in wurtzite GaN [6] Optical transitions occur at the Γ-point region

1 The structural properties as obtained by X-ray diffraction and in particular such measures as the half-width of the rocking curves

2 The electrical properties as given by the electron and hole concentrations and mobilities

3 The luminescent properties as measured by the ratio of near-bandgap excitomc recombination with respect to deep level emission at low temperatures and the small half width of the excitonic recombination lines

The main problem with GaN technology is that it suffers from a lack of a convenient lattice-matched substrate for epitaxy leading to mismatched heteroeptitaxial growth Epitaxial growth of GaN is usually performed on sapphire (Al_2O_3) However, sapphire is lattice mismatched to GaN by 13 8% [7] Both the lattice and thermal expansion coefficient mismatch and non-ideal nucleation causes a high density of dislocations in the range $10^{10}cm^{-2}$ [10] and fault zones (defects) which can adversely affect luminescence in

semiconductors by providing non-radiative paths through which electrons can recombine with holes Typically these defects form deep levels in the middle of the gap that sequentially capture an electron and a hole resulting in the recombination energy dissipating into phonons [8] These non-radiative centres lower both the efficiency and decay time of the luminescence Some of these issues can be alleviated by the introduction of a buffer layer of a few nm's of AlN or GaN deposited at low temperatures ($\approx 500^{o}$C) A detailed discussion of growth methods is provided by Orton *et al* [9]

3.4 N and P Type Dopants in GaN

The formative stage of any semiconductor device technology requires the selection and characterisation of dopants Both impurities and native defects may act as donors and acceptors and affect the electrical conductivity of semiconductors The dopant species is chosen to achieve the desired device performance and the controlled introduction of the dopant is required for reproducible characteristics Nominally undoped GaN shows a residual n-type doping at a level thought to be 1×10^{17}cm^{-3} [10] Controlled n-type doping is achieved with Si which substitutes for Ga in the GaN lattice P-type doping has been successfully achieved using magnesium (Mg), however the associated levels are deep (250meV [11][12]) and higher hole concentrations are desirable to limit series resistance and give better ohmic contacts [13] Using magnesium the associated acceptor level of 250meV is only partially ionised thus a higher dopant level is required to achieve a sufficient carrier concentration at room temperature This increase in dopant level also increases other impurities and reduces crystal quality An alternative approach is to use an impurity which forms a shallower level in the bandgap This results in a higher hole concentration without the need for a high dopant level It is the motivation of this study to investigate a shallower acceptor species Beryllium (Be) has been proposed as a suitable canditate [14][15], with theory indicating an ionisation energy of 60meV [16] This value is much smaller than any observed acceptor binding energies which range from 90meV [15]

to 150meV [7] For p-type dopants, two main factors determine acceptor incorporation

1 Strength of chemical bond between the acceptor and its neighbours

2 Atomic size match between acceptor and host atom for which it substitutes

Chapter 5 presents results of Be implanted GaN and compares the photoluminescence spectra with published results

A PL study of Au implanted GaN is also presented It has been found using Si technology that the most effective carrier traps lie near the centre of the bandgap These impurity centres are an important means of electron and hole recombination in indirect bandgap semiconductors where direct recombination of an electron with a hole across the bandgap is a rare event The introduction of Au ions into the Si lattice produces such centres These centres remove carriers by trapping a hole and an electron thus removing an electron-hole pair in the process and are referred to as 'lifetime killers' [17] This has benefits for devices such as the speeding up of a transistor by reducing the minority carrier lifetime in the base region of a bipolar transistor This study of Au implanted GaN aims to determine whether deep centres are observed in PL spectra

References

[1] Orton & Foxon, Group III nitride semiconductors for short wavelength light-emitting devices, Rep Prog Phys 61, (1998), pp 22

[2] Orton & Foxon, Group III nitride semiconductors for short wavelength light-emitting devices, Rep Prog Phys 61, (1998), pp 5

[3] Varshni Y , Temperature dependence of the energy gap in semiconductors, Physica 34 (1967), pp 149-154

[4] Mah *et al*, Defect luminescence of GaN grown by pulsed laser deposition, Journal of Crystal Growth 222, (2001), pp 497-502

[5] Gil B , Group III Nitride Semiconductor Compounds, Defect Spectroscopy in the Nitrides (Meyer *et al*, Oxford University Press, 1998), pp 242

[6] Pearton S , GaN and Related Materials II, Vol 7, (Amsterdam Gordon & Breach, Optolectronic properties of semiconductors and superlattices, 2000), pp 268

[7] Gil B , Group III Nitride Semiconductor Compounds, Beyond Silicon The rise of Compound Semiconductors (O'Donnell, Oxford University Press, 1998), pp 13

[8] Gil B , Group III Nitride Semiconductor Compounds, Beyond Silicon The rise of Compound Semiconductors (O'Donnell, Oxford University Press, 1998), pp 17

[9] Orton & Foxon, Group III nitride semiconductors for short wavelength light emitting devices, Rep Prog Phys 61, (1998), pp 12

[10] Monemar B , Basic III-V nitride research - past, present and future, Journal of Crystal Growth 189/190 (1998), pp 1-7

[11] Orton J , Acceptor binding energy in GaN and related alloys, Semicond Sci Technol 10 (1995), pp 101-104

[12] Fischer *et al*, On p-type doping in GaN - acceptor binding energies, Appl Phys Lett 67 (9), (1995)

[13] Neugebauer *et al*, Chemical trends for acceptor impurities in GaN, Appl Phys Lett (85-5) (1999), pp 3003

[14] Salvador A , Near ultraviolet luminescence of Be doped GaN grown by reactive molecular beam epitaxy using ammonia, Appl Phys Lett 69 (18) (1996)

[15] Sanchez *et al*, Luminescence of Be-doped GaN layers grown by molecular beam epitaxy on Si (111), MRS Internet J Nitride Semicond Res 3, 19 (1998)

[16] Bernardim *et al*, Theoretical evidence for efficient p-type doping of GaN using beryllium, Appl Phys Lett 70 (2), (1997)

[17] Parker G , Introductory Semiconductor Device Physics, (Prentice Hall, 1994), pp 67

4 Photoluminescence System

4.1 Introduction

This chapter provides a description of the various equipment elements used in the characterisation of GaN samples using photoluminescence Spectrometer details, laser excitation source, detector characteristics and cryostat equipment are presented

4.2 Photoluminescence Theory

Photoluminescence (PL) spectroscopy is an essential tool for the investigation of optical processes within semiconductor samples If a sample is excited by a laser with an energy greater than the bandgap then an excess of electron-hole pairs is created These can recombine through various recombination paths available, some emitting a photon of energy $h\nu$, see figure 5 In photolummescence spectroscopy, measurements are made of optical emissions from the sample as electrons return to the ground state This optical signal is dispersed to provide an intensity versus wavelength spectrum

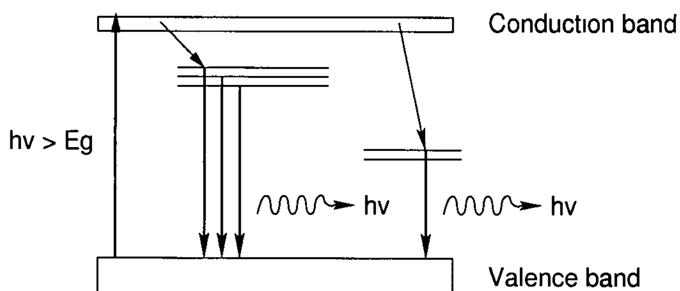

Figure 5 Conventional photoluminescence where excitation is performed above the bandgap and the resulting luminescence is a result of various recombination channels due to the presence of defects and impurities

4.3 Experimental System

An illustration of the equipment used in photoluminescence spectroscopy is provided in figure 6 The main elements of the system are laser excitation source, continuous flow cryostat, grating spectrometer and computer acquisition

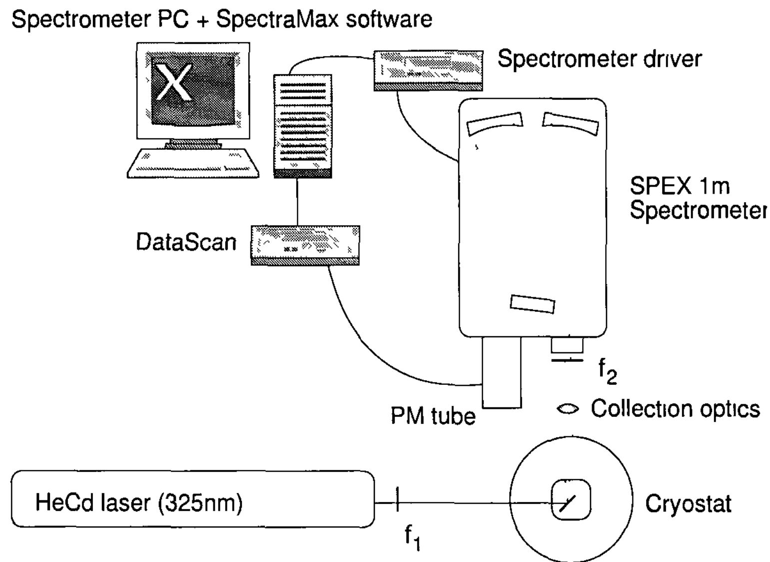

Figure 6 Conventional PL arrangment using a dispersive grating spectrometer Excitation is performed above the bandgap

4.3.1 Laser Excitation Source

The HeCd laser (OmniChrome model 3056-M-AΦI) operating at 325nm (3 825eV) was used to excite the GaN samples with an output power of 22mW In figure 6, filter f_1 is used to block laser plasma emission and ensure that only the UV line (325nm) is transmitted to excite the sample Filter f_2 prevents the 325nm line from reaching the spectrometer while allowing all other luminescence to pass

4.3.2 Spectrometer

The study presented in this thesis used a grating based monochromator (model SPEX 1704) to collect and disperse the optical signal This is a

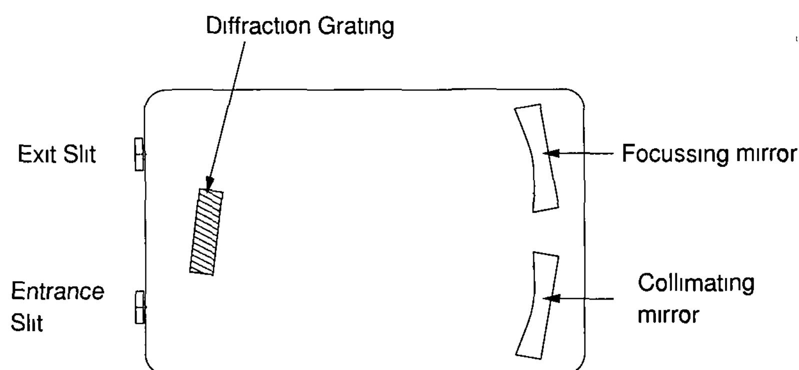

Figure 7 The Czerny-Turner is one of the most common monochromator configurations Luminescence from the sample passes through the entrance slit where it is reflected by a collimating mirror and spatially separated by a diffraction grating The angle of the grating discriminates between the wavelengths reaching the exit slit

1 metre focal length spectrometer employing two concave mirrors of 100mm diameter and a ruled diffraction grating in a Czerny-Turner configuration, see figure 7 A detailed account of spectrometry is provided in the ISA manual [1] Important aspects of monochromator performance such as dispersion, resolving power, bandpass and resolution are described in this manual The resolution is a particularly important parameter when investigating spectra obtained from a monochromator The resolution, R, of a grating monochromator is a measure of its ability to separate two closely spaced spectral lines The Rayleigh criterion states that two wavelengths, λ_1 and λ_2, are resolved if the central maximum of one line falls on a diffraction minimum of the other [2] and is expressed as

$$R = \frac{\lambda}{\Delta\lambda} \tag{5}$$

In practice the resolution depends on parameters like the resolving power of the grating, system focal length and slit width A practical definition for the

resolution of a spectrometer is the full width at half maximum (FWHM) of a single monochromatic spectral line [3]

The grating used for the visible region was a 330nm blazed ruled diffraction grating with 1200 grooves/mm (ISA model 510-05) This grating was used for the spectral range 320nm-600nm Au implanted GaN samples exhibited PL features in the range 355nm to 900nm and required another grating specifically blazed in the infrared region which had a groove density of 1000 grooves/mm The grating is automatically controlled using the SpectraMax (ISA) software

4.3.3 Photomultiplier Detector

The resulting luminescence dispersed by the spectrometer was detected using a cooled (-25°C) photomultiplier (PM) tube The PM tube (Hamamatsu model R3310-02) is configured for photon counting and has a wide spectral range (300nm-1040nm) The PM incorporates an InGaAs (Cs) photocathode, and linear focused CuBeO dynodes Detector performance is described using the following terms, responsivity (R), Noise Equivalent Power (NEP), Detectivity (D), Dark Current and Quantum Efficiency (QE)

The responsivity is defined as the output voltage or current per watt of incident signal when noise is not a consideration and is given by

$$R = \frac{S}{PA} \qquad \text{(V/W) or (A/W)} \tag{6}$$

where S is the signal output voltage (V) or current (A), P is the incident energy (W/cm^2) and A is the sensitive area of detector (cm^2)

The Noise Equivalent Power (NEP) represents the lower detection limit of a detector It is expressed as the quantity of incident light intensity equal to the quantity of intrinsic noise, i e the quantity of incident light when the signal to noise ratio (S/N) becomes unity Since the S/N ratio is proportional to the square root of the bandwidth, the NEP is given by

$$NEP = \frac{PA}{\frac{S}{N}\sqrt{\Delta f}} \qquad \text{W}/\sqrt{Hz} \tag{7}$$

where N is the noise output in Volts and f is the noise bandwidth in Hz The detectivity (D) is simply the reciprocal of the Noise Equivalent Power

The Dark Current is the output current which flows even when input radiation is absent or negligible For our photomultiplier tube the equivalent anode dark current is quoted as 5nA [4]

For a detector, quantum efficiency (QE) is defined as the ratio of induced current to incident flux The quantum efficiency depends on the energy of the impinging photon, the material shape, size and other physical parameters such as the thickness and reflectivity of the surface For example at a wavelength of 253 7nm the quoted quantum efficiency for our PM tube is 15%

Figure 8 shows both the photomultiplier tube efficiency curve and the visible grating efficiency curve Equations representing these curves are presented in Appendix A

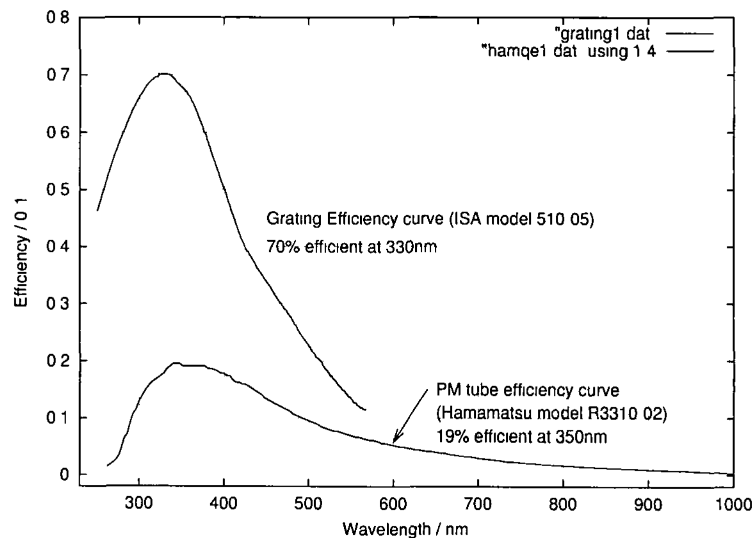

Figure 8 Efficiency curve for Hamamatsu photomuliplier tube and grating blazed for visible region

4.3.4 Continuous Flow Cryostat

The sample is enclosed in a continuous flow cryostat for controllable temperatures down to 4 2K A continuous and controlled flow of coolant, namely liquid He, passed through the heat exchanger of the cryostat where the temperature was measured and a resisitive heater connected to a temperature controller maintained the desired temperature The cryostat was enclosed in a vaccum jacket to ensure thermal insulation These low temperatures are desirable to reduce the thermal broadening of the excited carrier energies, which at temperature T is roughly k_bT [5] This gives a significant broadening of 25meV at 300K and reduces to $<$ 1meV at 10K Cooling produces sharper and more readily defined peaks and tends to reduce the role of competing nonradiative paths for recombination, giving a higher efficiency for the PL process which results in an improved signal to noise ratio Cooling also prevents impurity centres from undergoing thermal ionisation

4.4 System Calibration

Calibration for a PL spectroscopic system is essential to ensure accuracy at high resolution and to provide a correction curve for all spectra obtained System calibration curves are presented for each grating used For Au implanted GaN, a grating blazed for the infrared region is used and for Be implanted GaN, a grating designed for the visible region is used When a new grating is installed in the SPEX spectrometer, realignment is usually necessary and consists of a procedure referred to as 'rocking the grating' [6] It is only necessary to perform this once as the grating mount retains its calibration settings Perfect calibration at both high and low wavelengths is difficult to achieve so a compromise is met in the form of a calibration curve

For the grating used in the visible spectral region, a linear fit on the calibration curve (see figure 10) allows for minor corrections at each wavelength, particularly for sharp lines in the spectra A mercury discharge lamp was used for this purpose The mercury lamp spectra can be seen in figure 9

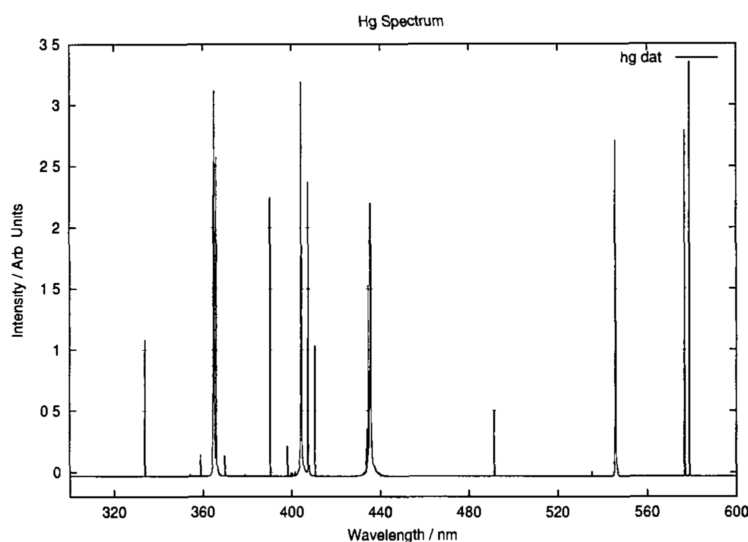

Figure 9 Hg spectrum obtained using a grating blazed for visible region

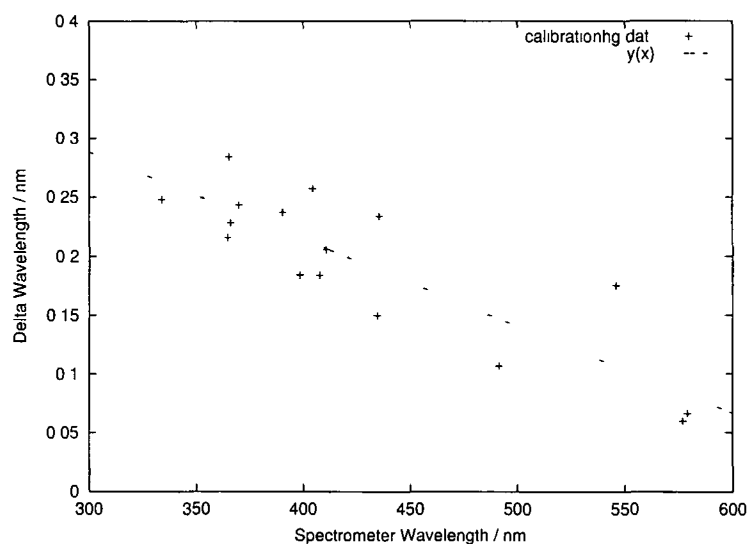

Figure 10 Calibration curve for grating blazed for visible region Graph compares known lines of a Hg discharge lamp with values obtained from the spectrometer The linear fit illustrated, $y = mx + c$ is $y = -0\ 00073817x + 0\ 50955$, thus, for example, a reading of 410 6nm on the spectrometer is actually 410 6nm + 0 206nm = 410 806nm

Similarly, for the grating used in the infrared spectral region, the Hg lamp spectra are presented in figure 11 A calibration curve is shown in figure 12

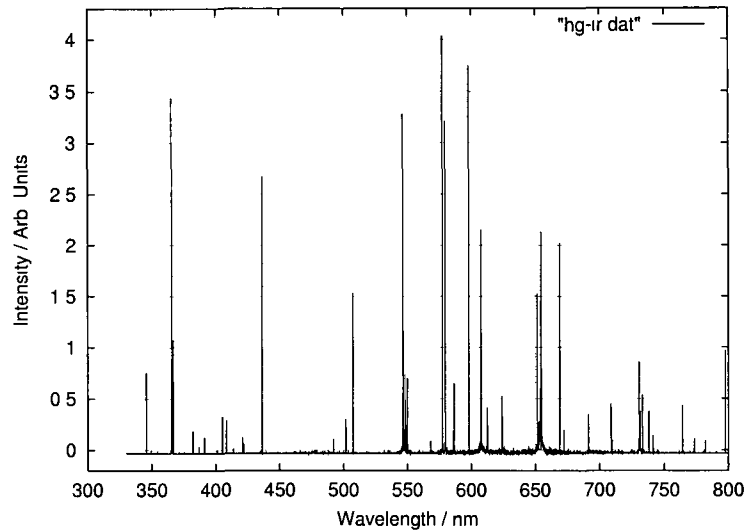

Figure 11 Hg spectrum obtained using a grating blazed for infrared region

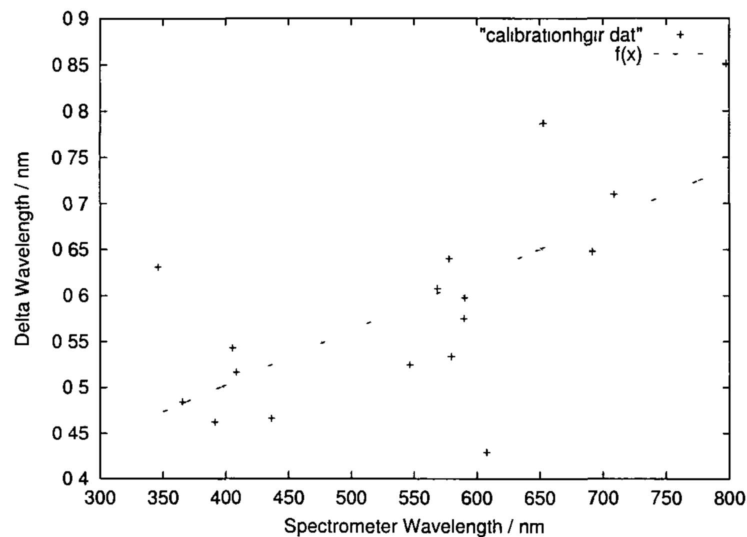

Figure 12 Calibration curve for grating blazed for infrared region Graph compares known lines of a Hg discharge lamp with values obtained from the spectrometer The linear fit illustrated, $y = mx + c$ is $y = 0\ 00059047x + 0\ 26693$, thus, for example, a reading of 546 6nm on the spectrometer is actually 546 6nm + 0 589 = 547 189nm

References

[1] ISA Jobın-Vyon SPEX, Guıde for Spectroscopy, pp 36

[2] Gılchrıst J , Spectroscopy The Tools of the Trade, (Photonıcs Desıgn and Applıcatıons Handbook, 2000) pp H-81

[3] CVI Spectral Products, Spectrometer Basıcs

[4] Hamamatsu R3310-02 Photomultıplıer Tube Spec Sheet

[5] Perkowıtz S , Optıcal Characterızatıon of Semıconductors, (Academıc Press London, 1993) pp 52

[6] SPEX model 1704 manual

5 Photoluminescence Results

5.1 Introduction

Photoluminescence results are presented for both Be and Au implanted GaN PL spectra of bare GaN, referred to as 'reference material', are shown prior to implantation with Be A temperature dependence study is performed on each Be implanted sample with a step size of 0 5nm and 0 2s integration time over a spectral range of 340nm to 690nm The spectrometer entrance and exit slits were a consistent 80μm All Be implanted GaN spectra are corrected against a system response curve PL spectra are shown for samples which are not annealed and samples which were annealed to investigate the effect of annealing on the removal of ion implantation damage and the optical activation of impurities

Photoluminescence results of Au implanted GaN is presented One sample was implanted at 1×10^{12} cm^{-2} and another at 1×10^{13} cm^{-2}

5.2 Sample Preparation

The bare, reference GaN material prior to Be implantation was obtained from a 2" GaN epilayer grown by MOCVD on sapphire (supplied by Emcore) Approximately 40 samples of size 5mm $\times$ 8mm were precisely cut out using a diamond saw The GaN is grown on a c-plane sapphire substrate with a single side polish and having a mean thickness of 430μm The GaN layer grown on this substrate has a layer thickness of 2 0μm (uniformity 5%) with a residual n-type doping at a level of $1\ 0 \times 10^{17}$ cm^{-3}

Be implantation was performed by Implant Sciences [1] Ion implantation was chosen as it allows easy and controlled introduction of virtually any dopant species The main features of this technique are

- The concentration as well as the lateral and depth distributions of the dopant(s) are precisely controllable
- Almost all elements can be implanted with sufficiently high purity

- Ion implantation is always accompanied by structural damage to the crystal lattice which requires thermal annealing to achieve electrical activation of the dopants

Samples were implanted at 150keV with three implantation levels, namely, $1 \times 10^{12}\text{cm}^{-2}$, $1 \times 10^{13}\text{cm}^{-2}$ and $1 \times 10^{14}\text{cm}^{-2}$, see table 1 Samples were annealed to remove ion implantation damage Annealing of the Be samples was done using two different methods For both methods, quartz ampoules were used to enclose the sample and provide the correct ambient pressure of nitrogen thereby ensuring stoichiometry The first method used 0 5 Atm N_2 at 1000°C for 10 minutes The second annealing method used elemental aluminium in the evacuated quartz ampoules at 1000°C for 10 minutes As detailed by Burchard [2] on Cd implanted GaN, due to the vapour pressure of elemental aluminium at high temperatures a protective layer forms on the GaN surface which effectively suppresses both the loss of N and Cd This is the method tested here on Be implanted GaN

Sample ID	**Implantation Dose**	**Annealing Treatment**
GaNBe1201	$1 \times 10^{12}\text{cm}^{-2}$ @ 150keV	0 5Atm N_2 at 1000°C / 10 mins
GaNBe1202	$1 \times 10^{12}\text{cm}^{-2}$ @ 150keV	Vaccum with Al @ 1000°C / 10 mins
GaNBe1203	$1 \times 10^{12}\text{cm}^{-2}$ @ 150keV	Not Annealed
GaNBe1301	$1 \times 10^{13}\text{cm}^{-2}$ @ 150keV	0 5Atm N_2 @ 1000°C / 10 mins
GaNBe1302	$1 \times 10^{13}\text{cm}^{-2}$ @ 150keV	Not Annealed
GaNBe1303	$1 \times 10^{13}\text{cm}^{-2}$ @ 150keV	Vaccum with Al @ 1000°C / 10 mins
GaNBe1401	$1 \times 10^{14}\text{cm}^{-2}$ @ 150keV	0 5Atm N_2 @ 1000°C / 10 mins
GaNBe1402	$1 \times 10^{14}\text{cm}^{-2}$ @ 150keV	Not annealed
GaNBe1403	$1 \times 10^{14}\text{cm}^{-2}$ @ 150keV	Not annealed

Table 1 Implantation dose and annealing treatment of Be implanted GaN samples

5.3 Be Impanted GaN

Temperature dependent photoluminescence spectra of the unimplanted GaN material, referred to as 'reference material', are illustrated in figure 13 At low temperatures, this material appears to be of good quality and exhibits strong band edge luminescence at 3 488eV (at 4 3K) with LO phonons observed A detailed investigation at higher resolution is presented in figure

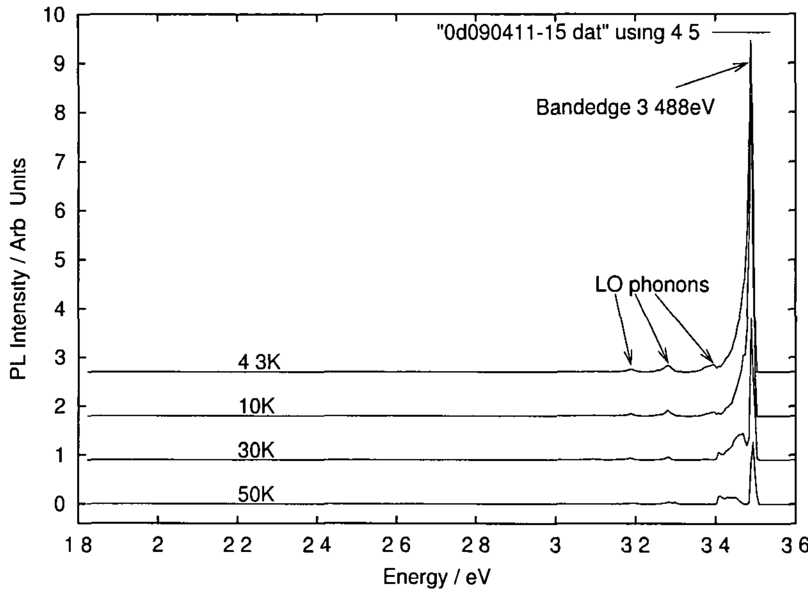

Figure 13 Undoped GaN as supplied by Emcore prior to implantation with Be Excitonic transitions and LO phonon replicas are identified in a higher resolution spectrum in figure 14

14 Viswanath *et al* [3] presented a study of excitomc transitions in undoped GaN epitaxial layers and observes free exciton lines FX[A] and FX[B], donor bound exciton (DX) and LO phonon replicas The free exciton, FX[A] was better resolved in the study by Viswanath, however, our investigation seen in figure 14 shows it to be enveloped by the donor bound exciton, DX Close investigation reveals a free exciton FX[B] at 3 504eV smothered by FX[A] (at 3 498eV) The separation between these energy levels, ΔE_{AB}, is 6meV m agreement with the theoretical value determined by band structure calculations [4] The phonon assisted excitonic transitions located in the region of

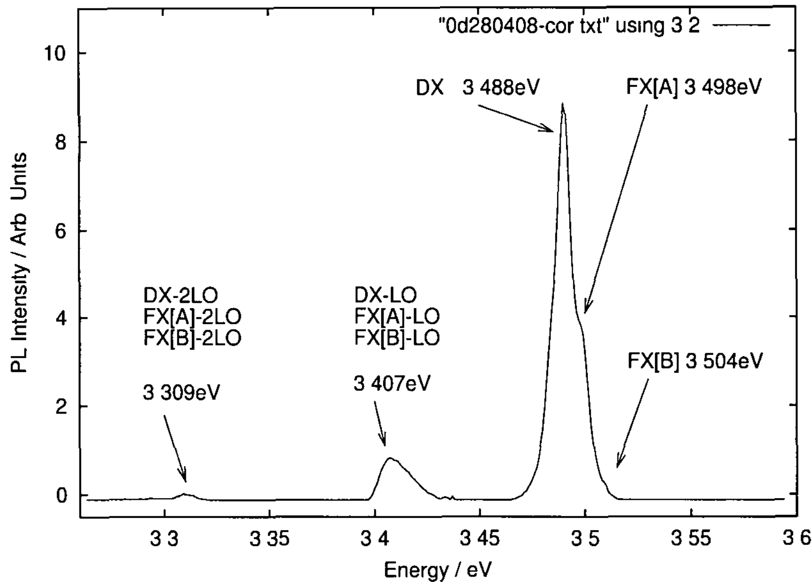

Figure 14 Higher resolution spectrum of figure 13 at 10K Free excitons, FX[A] and FX[B] and donor bound exciton DX are illustrated along with phonon assisted exciton transitions

3 407eV were also seen by Viswanath and by fitting three Lorentzian peaks were assigned to the phonon assisted transitions of DX, FX[A] and FX[B] From figure 14 the separation of the 3 407eV peak from DX, FX[A] and FX[B] is 81meV, 91meV and 97meV respectively These values are within the region of the known LO phonon energy of 92meV for GaN Contained within this band is a series of multiple overlapping peaks representing the individual phonon energies A higher resolution study would confirm the energies of these phonon replicas A second order series of phonon replicas, DX-2LO, FX[A]-2LO and FX[B]-2LO is also observed at lower intensity at approximately 3 309eV

The low temperature spectrum in figure 13 shows no 'yellow luminescence', however, at room temperature this band dominates the spectrum This strong luminescence band observed at 2 2eV is a defect induced transition and its presence m GaN is often regarded a sign of poor quality material Native defects or residual impurities have been proposed as candidates for

the origin of the electronic level(s) participating in this band [5] Neugebauer *et al* attributed this parasitic effect to gallium vacancies [6] The ratio of the bandedge luminescence to this yellow band is often taken as a sign of the quality of the GaN It was noted that some low temperature photoluminescence spectra of samples implanted with Be exhibit yellow luminescence possibly as a result of ion implantation damage

As previously mentioned in section 3 4, the motivation for studying Be implanted GaN is to verify whether Be forms a shallower acceptor state than other elements currently used to obtain P-type GaN Mg has been successfully used to create P-type GaN with an acceptor ionisation energy of 250meV This is a rather deep level and requires a higher implantation dose to achieve a sufficient carrier level acceptable for device operation A number of studies of Be implanted GaN have been performed with some promising results The aim in this thesis is to generate a set of data for comparison with previous studies

Ronning [7] reports a band in Be implanted GaN at 3 35eV and assigns it to a band-acceptor recombination with an ionisation energy of 150meV $\pm$ 10meV This is approximately twice the value calculated by Bernardini [8] and only appeared following annealing at 600°C Dewsnip *et al* [9] also observed a new line in GaN samples doped with Be during growth at 3 385eV and calculated the ionisation energy to be 90-100meV on the assumption that this line is a donor-acceptor transition Other sources confirm Be as forming a shallow acceptor state in GaN [10]

5.3.1 Be Implanted GaN at $1 \times 10^{12}\mathrm{cm}^{-2}$

Strong band edge luminescence (at approximately 3 45eV) is seen for all samples implanted at $1 \times 10^{12}\mathrm{cm}^{-2}$ It can be seen by comparing figure 15 with figures 16 and 17 that an annealing step is required for the optical activation of a band located around 3 3eV to 3 4eV This band is located at 3 4eV for the N_2 annealing step (figure 16) and is shifted to 3 35eV for the Al annealing step (figure 17) For the Al annealing step stronger luminescence is seen at 3 35eV compared with the N_2 annealing step It may be possible that the Al capping layer prevents Be diffusing out during annealing thus preserving the stoichiometry

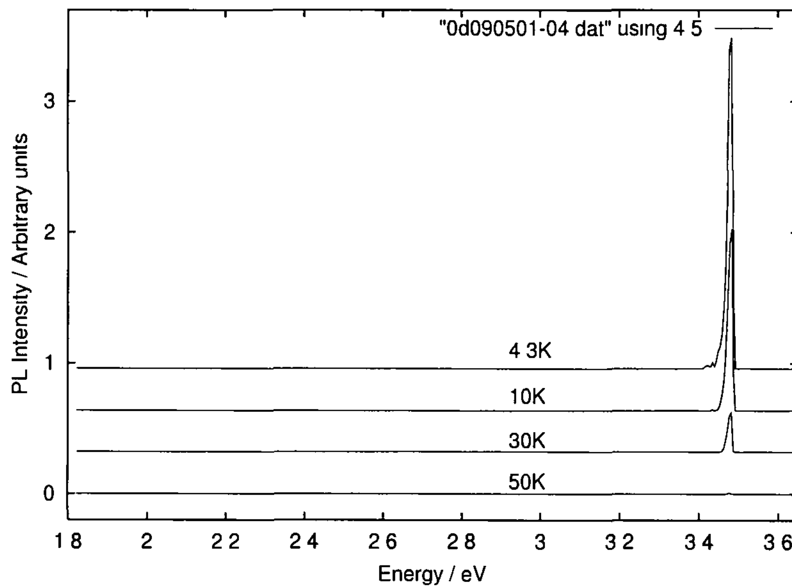

Figure 15 GaN implanted with Be at $1 \times 10^{12}\mathrm{cm}^{-2}$ at 150keV No annealing step was taken Sample ID = beganl203

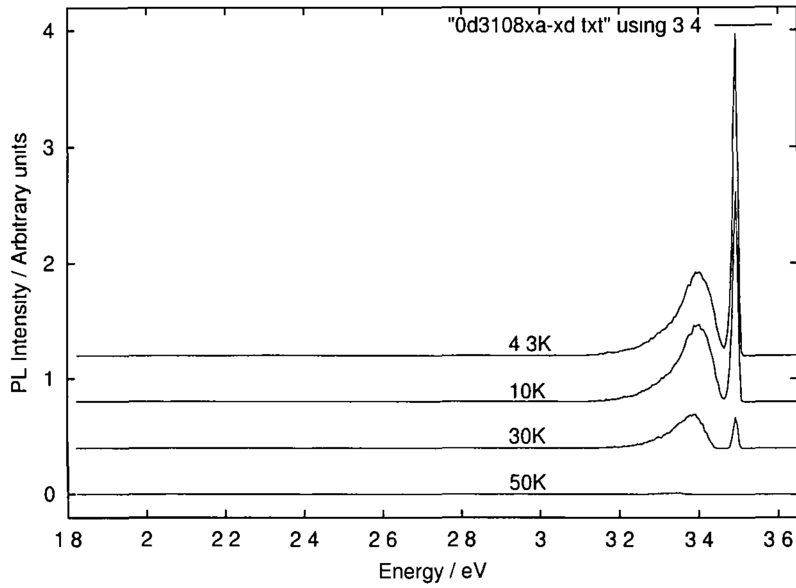

Figure 16 GaN implanted with Be at 1×10^{12}cm^{-2} at 150keV and annealed in 0 5 Atm of N_2 at 1000°C for 10 minutes Sample ID = began1201

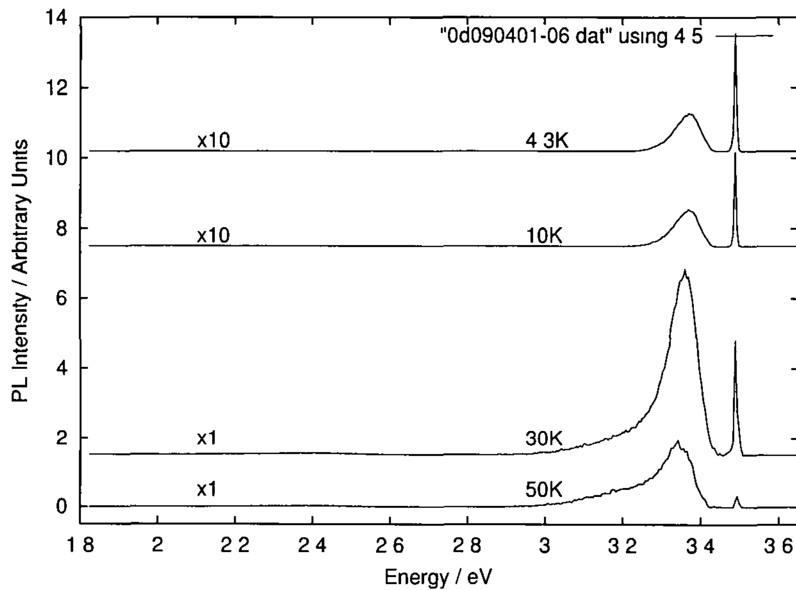

Figure 17 GaN implanted with Be at 1×10^{12}cm^{-2} at 150keV and annealed in vaccum with elemental Al at 1000°C for 10 minutes Sample ID = began1202

An ınterestıng result ıs seen when the PL spectrum ın figure 17 ıs repeated 15 months later (see figure 18) The bandedge lumınescence at 3 45eV ıs no longer seen In addıtıon, the band centered around 3 3eV to 3 4eV remaıns although at much lower ıntensıty and an ıncrease ın the band centered at 2 3eV ıs seen It may be possıble that Be dıffused out from the sample over a perıod of 15 months due to ıts small atomıc sıze and ıts storage at room temperature

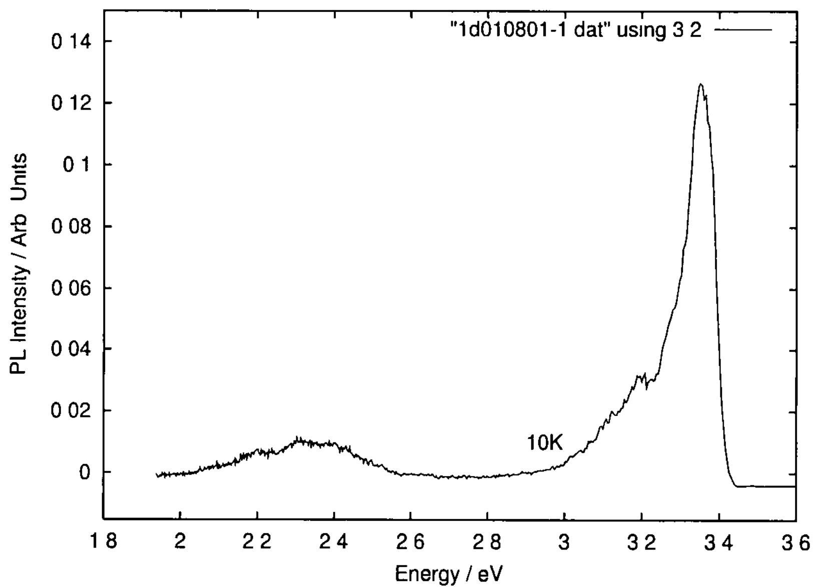

Fıgure 18 Repeat of PL spectrum of figure 17 at 10K 15 months later

5.3.2 Be Implanted GaN at 1×10^{13}cm^{-2}

Prior to annealing, the overall luminescence signal in figure 19 is quite weak However, following an annealing step, an increase in 'yellow luminescence' is observed at 2 45eV (figures 20 and 21) This may be due to increased lattice damage at the higher implantation level A stronger PL signal is seen in the sample annealed with an Al capping layer (figure 21) The most notable feature resulting from the annealing step is the optical activation of the band located around 3 3eV (figures 20 and 21), this compares well with the samples implanted at 1×10^{12}cm^{-2} The bandedge luminescence in these samples is much weaker when compared with samples implanted at 1×10^{12}cm^{-2} and is possibly attributed to increased lattice damage at the higher implantation dosage

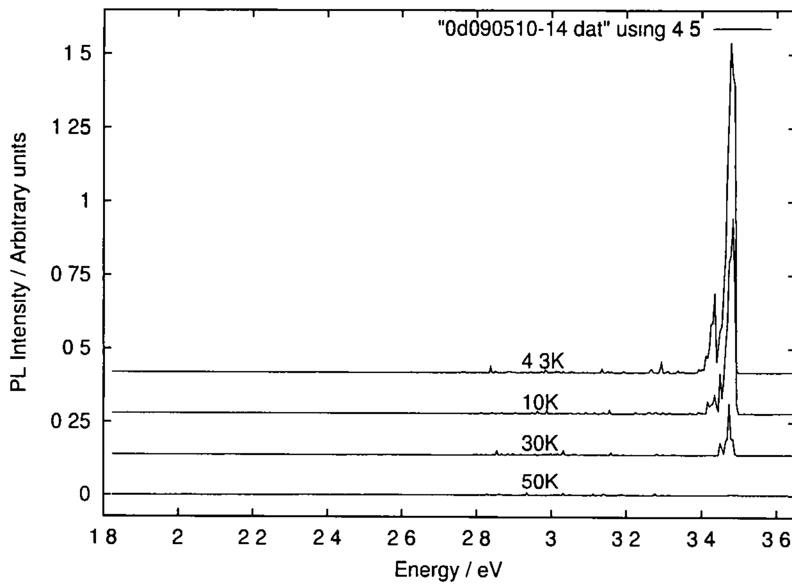

Figure 19 GaN implanted with Be at 1×10^{13}cm^{-2} at 150keV This sample is not annealed Sample ID = began1302

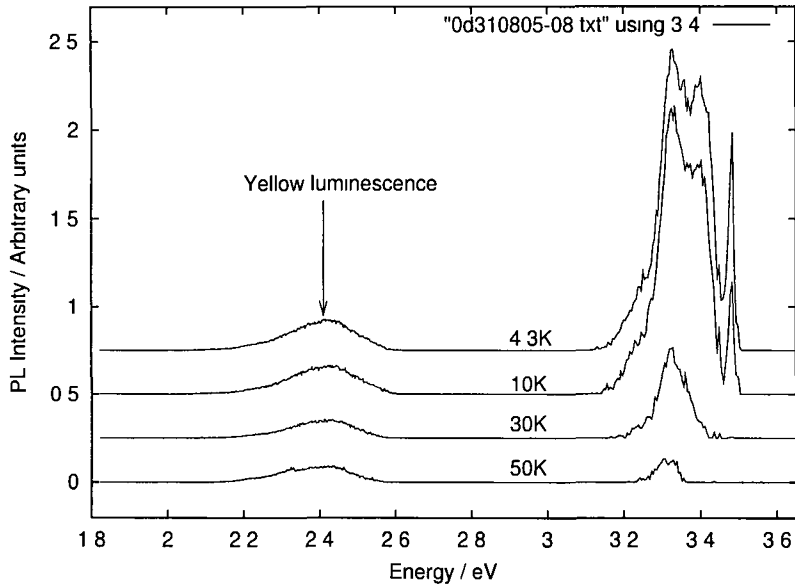

Figure 20 GaN implanted with Be at $1 \times 10^{13}\mathrm{cm}^{-2}$ at 150keV and annealed in 0 5 Atm of N_2 at 1000°C for 10 minutes Sample ID = began1301

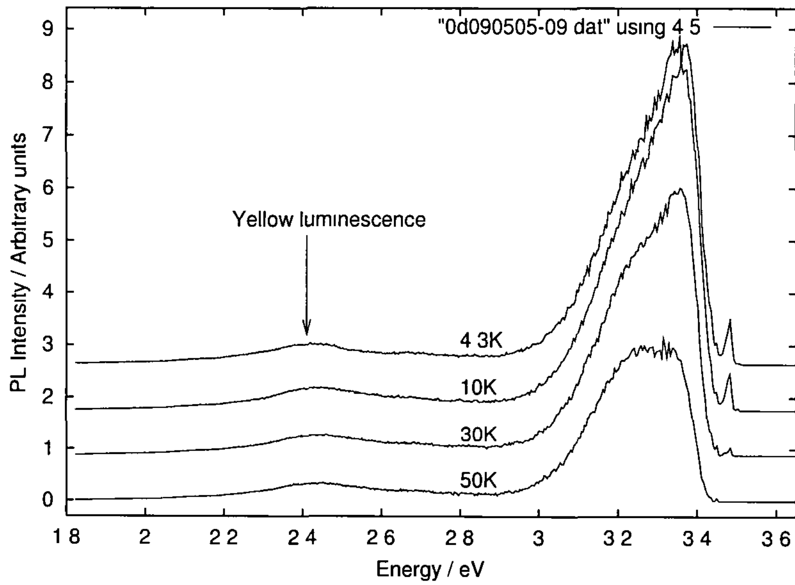

Figure 21 GaN implanted with Be at $1 \times 10^{13}\mathrm{cm}^{-2}$ at 150keV and annealed in vaccum with elemental Al at 1000°C for 10 minutes Sample ID = began1303

5.3 3 Be Implanted GaN at $1 \times 10^{14}\text{cm}^{-2}$

Strong bandedge luminescence is observed for samples implanted with Be at $1 \times 10^{14}\text{cm}^{-2}$ Annealing in a N_2 atmosphere activates a broad band at 2 4eV However, in the sample not annealed (figure 22) a band at approximately 3 3eV is seen This band is not observed in other samples which did not receive an annealing step It may be possible that due to the higher temperatures and currents required for this implantation level that a form of annealing took place which activated this band The annealing step in a N_2 atmosphere appears to reduce the intensity of this band (see figure 23), possibly due to over annealing which resulted in Be atoms diffusing out from the GaN lattice This Be related band is weaker than that for the lower implantation steps An annealing step using an Al capping layer was not performed

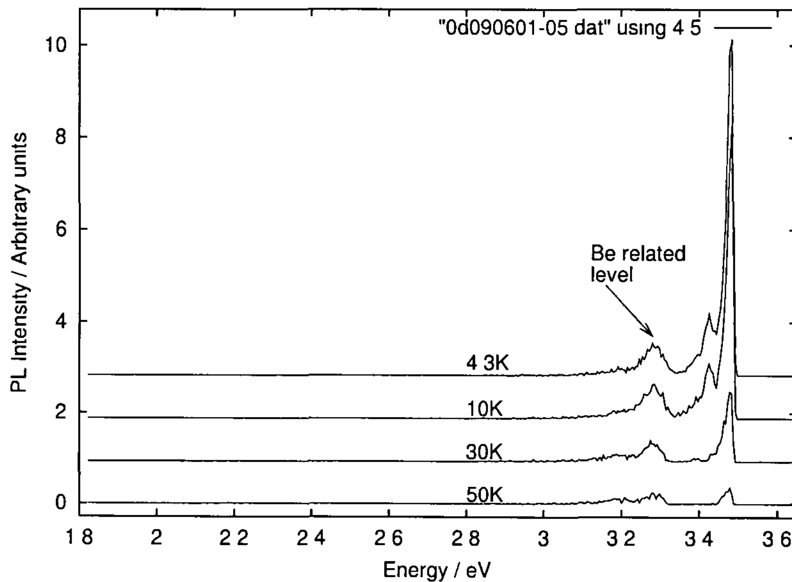

Figure 22 GaN implanted with Be at $1 \times 10^{14}\text{cm}^{-2}$ at 150keV Sample is not annealed Sample ID = began1403

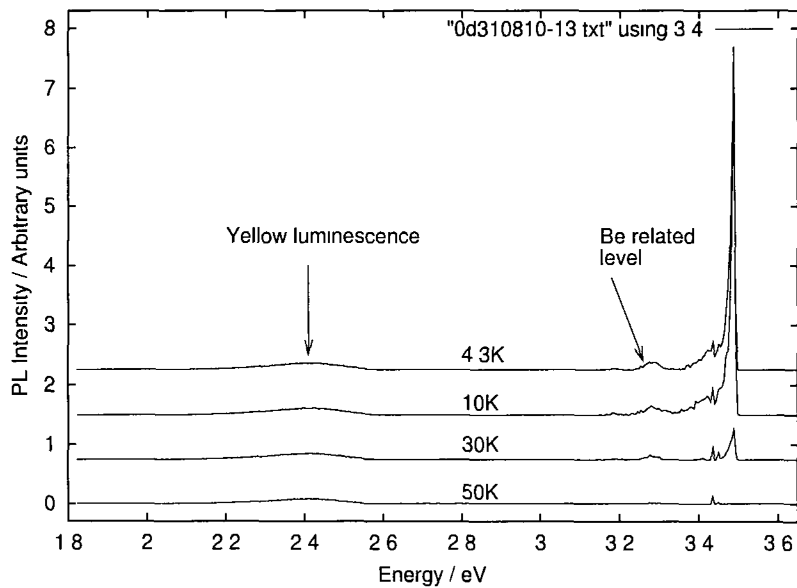

Fıgure 23 GaN ımplanted wıth Be at 1×10^{14}cm^{-2} at 150keV and annealed ın 0 5 Atm of N_2 at 1000°C for 10 mınutes Sample ID = began1401

5.4 Discussion

It can be concluded that Be implanted GaN produces a band located at 3 35eV-3 4eV An annealing step is required for the optical activation of this band The use of an Al capping layer during annealing appears to prevent Be diffusing out thus resulting in a stronger Be related band The strongest luminescence was seen for Be implanted at the lower implantation dosage of $1 \times 10^{12}cm^{-2}$ Higher implantation doses appeared to increase lattice damage (noted by an increase in the yellow luminescence band) Figure 24 illustrates these effects The Be related band at approximately 3 35eV is reduced in intensity at higher implantation levels, possibly as a result of increased implantation damage

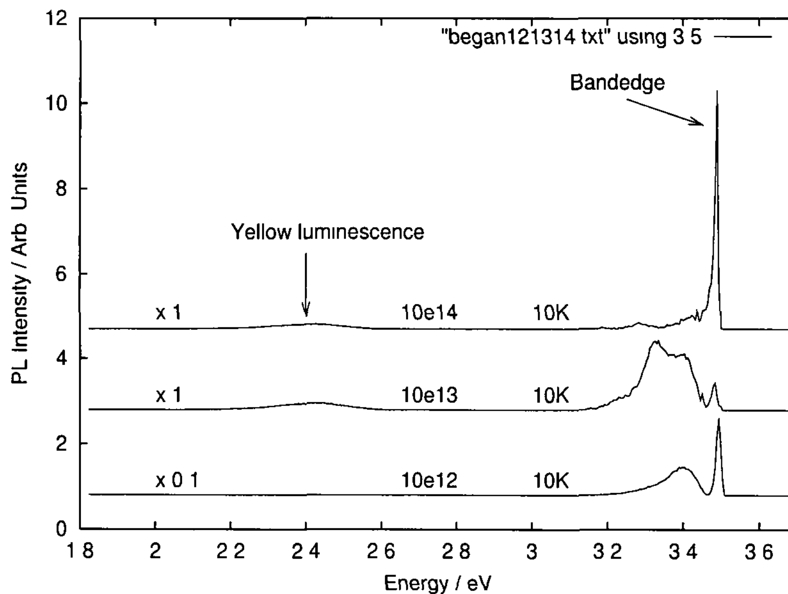

Figure 24 Combined PL spectra of the three implantation levels at $1 \times 10^{12}cm^{-2}$, $1 \times 10^{13}cm^{-2}$ and $1 \times 10^{14}cm^{-2}$ at 10K and annealed in N_2 Note the PL intensity for the $1 \times 10^{12}cm^{-2}$ implantation level is 10 times greater than the other two levels

An attempt was made to identify the nature of the recombination mechanism(s) involved in the band attributed to Be ions As previously mentioned, Be is reported to behave as an acceptor in GaN Possible recombination meth-

ods include an acceptor bound exciton at a Be acceptor or a donor to acceptor transition between the residual n-type doping and a Be acceptor The first possibility is tested using Haynes rule [11] which states that exciton binding energies of approximately 0 1E_A can be expected for excitons bound to neutral acceptors For the Be related defect this gives a hole ionisation energy of approximately 1500meV which is much deeper than other known acceptors (e g 250meV for Mg) and is an unlikely candidate as a recombination method The alternative recombination method, a donor to acceptor tran-

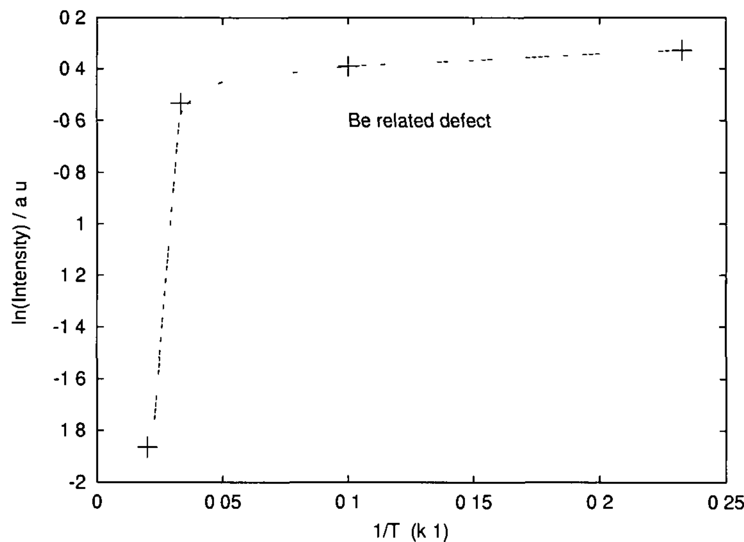

Figure 25 Temperature dependent intensities of the Be related band

sition, is investigated using temperature dependent intensity data Thermal data obtained from figure 16 was used to produce the temperature dependent intensity plot in figure 25 and shows a two slope behaviour related to the donor and acceptor ionisation energies A curve fit was generated using equation 8 to obtain estimates of the ionisation energies involved

$$I(T) = \frac{I_0}{1 + C_0 \times exp(-E_a/k_bT) + C_1 \times exp(-E_b/k_bT)} \qquad (8)$$

where $I(T)$ is the PL intensity at temperature T, C_0 and C_1 are the ratios of the degeneracy of the states to the degeneracy of the bands, I_0 is a constant,

k_b is Boltzmann's constant and E_a and E_b are the activation energies of the donor and acceptor respectively. Only the lower of the two activation energies will be obtainable from the temperature data. Below approximately 25K the slope changes to give an ionisation energy of 23meV which is close to the known donor binding energy of 27meV.

It can be seen in figure 26 that the Be related band shifts to lower energies with increasing temperature (indicated by arrows). In order to account for

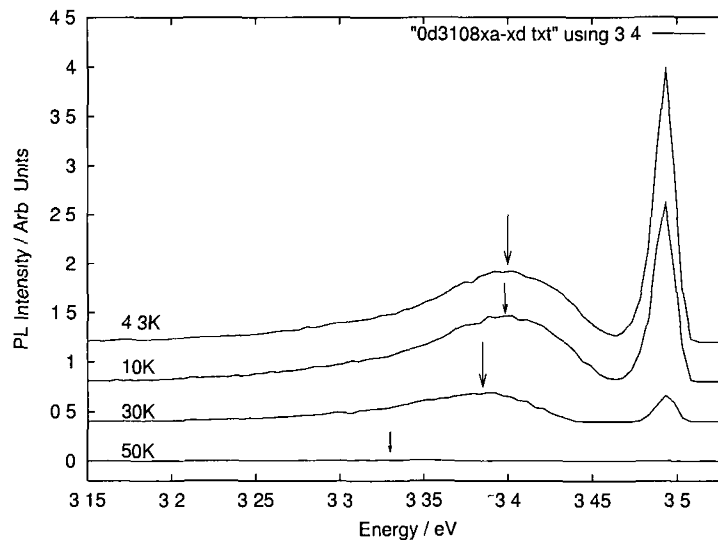

Figure 26 Magnified PL spectrum of figure 16 showing the effect of peak position with temperature

this behaviour the following model assumes that the Be related band is due to a donor to accceptor recombination with a single dominant donor and a range of acceptor defect levels being involved (illustrated in figure 27). Increasing temperature depopulates the shallower levels (e g. A1) with the trapped holes returning to the valence band leaving only the deeper levels, A2 and A3, available for transitions from the donor level. This effect is seen as a shift to lower energies of the Be related level (see figure 26) for a rise in temperature.

We can estimate the acceptor ionisation energy, E_A, by assuming that

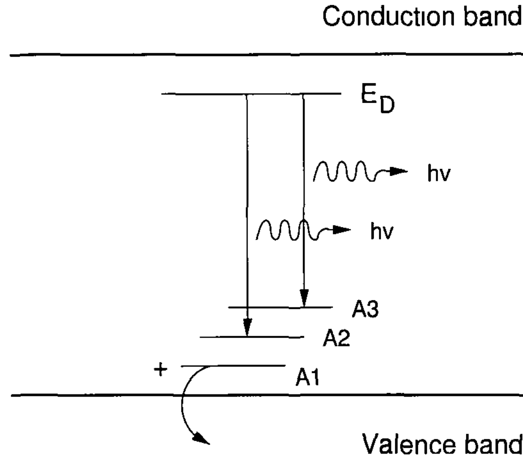

Figure 27 Model of the donor to acceptor transitions to explain the shift to lower energies with increasing temperature of the Be related band This model assumes a single dominant donor and a range of acceptor levels The spacing between acceptor levels is exaggerated for clarity

the photon energy is given by

$$hv = E_g - E_D - E_A \tag{9}$$

In this equation we ignore the Coulombic term which is particularly significant for adjacent DA pairs Taking the peak of the donor-acceptor band as 365nm, we get $hv \simeq 3\ 397eV$ For the equation above, with E_g = 3 503eV (at 10K) and E_D taken as 0 027eV (the accepted donor binding energy in GaN) we find E_A = 0 079eV This value, 79meV lies within the reported ionisation energy for Be of 60meV (theoretical) to 150meV (experimental) (as previously discussed) Using the same method but taking account for the coulombic interaction energy, Dewsnip *et al* estimated a Be acceptor energy of 90meV-100meV [9] In conclusion, it appears likely that Be forms a range of acceptor levels in GaN with the dominant form of recombination being a donor to acceptor pair

5.5 Au Implanted GaN

A brief photoluminescence study of Au implanted GaN was performed As previously published by Stotzler *et al* [12], implantation of GaN with Au ions produces many deep centres within the bandgap which emit photons at a wavelength requiring a grating blazed for the infrared spectral region The study by Stotzler et al involved the implantation of radioactive Hg ions which decay to Au A series of bands attributed to Au ions were seen in the spectral region 1 46eV to 1 77eV as well as a 'yellow luminescence' band at 2 2eV

These deep centres have proven to be an important impurity in Si technology where they act as lifetime killers thus enabling the speeding up of devices such as transistors Our study investigated the effect of Au impurities in GaN and involved a photoluminescence characterisation of Au implanted at $1 \times 10^{12}\text{cm}^{-2}$ and $1 \times 10^{13}\text{cm}^{-2}$ Both samples had different origins, the sample implanted at $1 \times 10^{12}\text{cm}^{-2}$ originated from Konstanz university in Germany and the sample implanted at $1 \times 10^{13}\text{cm}^{-2}$ originated from Portugal

For the sample implanted at $1 \times 10^{13}\text{cm}^{-2}$ (figure 28) a series of bands in the region 1 5eV to 2 4eV were observed The band stretching from 2 1eV to 2 2eV is often referred to as 'yellow luminescence' However, this band typically exhibits a Gaussian profile which is not observed here The peaks at 1 7eV and 2 3eV appear to be attributed to Au ions and are also seen in the GaN sample implanted at $1 \times 10^{12}\text{cm}^{-2}$ (see figure 29) In this sample the peaks are not readily observed until a temperature of 20K is reached The similarities between these peaks are interesting considering that both samples were acquired from different sources with unknown histories

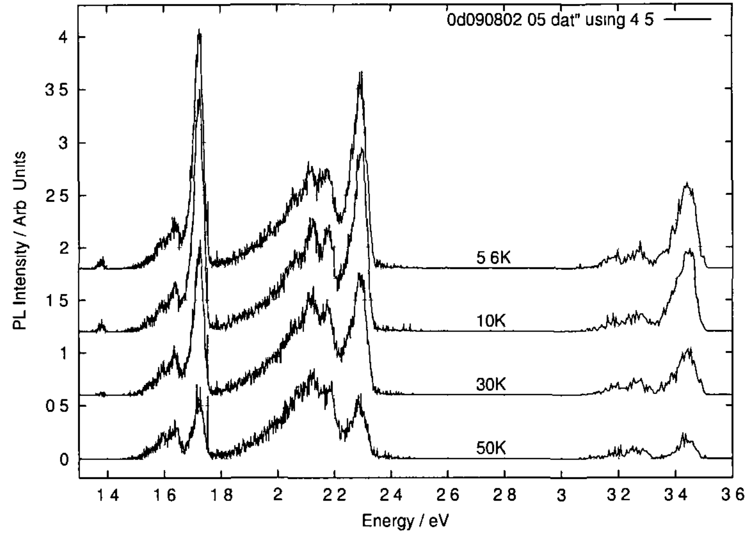

Figure 28 Au implanted GaN at $1 \times 10^{13}\text{cm}^{-2}$ at 160keV

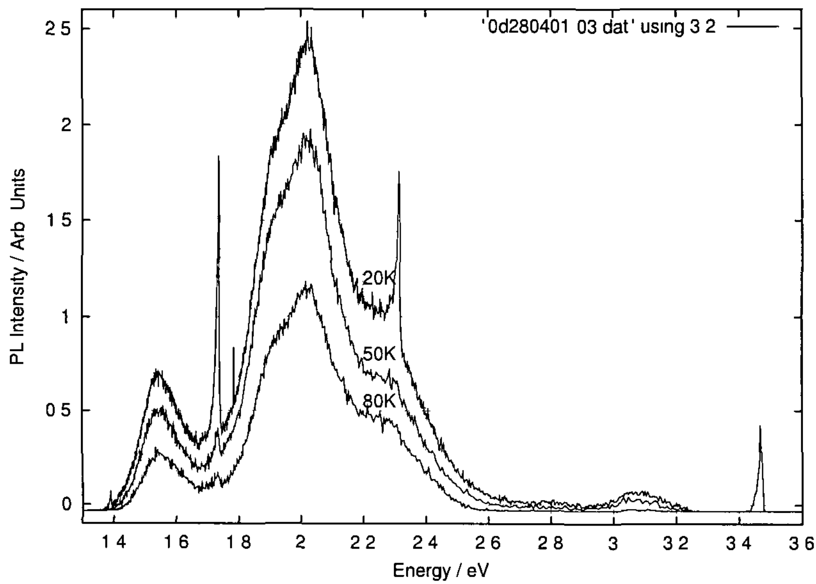

Figure 29 Au implanted GaN at $1 \times 10^{12}\text{cm}^{-2}$ at 160keV

5.6 Discussion

The implantation of Au ions into GaN causes a series of a deep centres located at approximately the centre of the bandgap which produce sharp lines and broad bands in the photoluminescence spectrum Although both samples originated from different sources and their full history was unknown, it can be seen that the peaks at approximately 1 7eV and 2 3eV appear consistently in both samples and these are attributed to Au impurities Several points should be noted concerning the details of the spectra in the two cases Firstly, the sample with the lower dose (figure 29) produces much sharper lines for both the band edge features and the Au-related features Furthermore, the dependence on temperature is more marked for the lower dose sample The likelihood is that the sample implanted with the higher dose (figure 28) is of poorer quality and that the defects produced by the implantation and annealing are more stable than is the case for the low dose sample

Further study of these peaks and bands would be useful to ascertain their effects on the lifetime of excited carriers

References

[1] Implant Scıences Corporatıon, 107 Audubon Road, Wakefield, MA 01880

[2] Burchard *et al*, Annealıng of ıon-ımplanted GaN, Physıca B 273-274 96-100 (1999)

[3] Vıswanath *et al*, Photolumınescence studıes of excıtomc transıtıons ın GaN epıtaxıal layers, J Appl Phys 84-7 (1998)

[4] Chen *et al*, Fundamental optıcal transıtıons ın GaN, Appl Phys Lett 68 (20) (1996)

[5] Suskı *et al*, Mechanısm of yellow lumınescence ın GaN, Appl Phys Lett 67 (15) (1995)

[6] Neugebauer *et al*, Gallıum vacancıes and the yellow lumınescence ın GaN, Appl Phys Lett 69 (4) (1996)

[7] Ronnıng *et al*, Optıcal actıvatıon of Be ımplanted ınto GaN, Appl Phys Lett , Vol 73-12 (1998), pp 1622

[8] Bernardını *et al*, Theoretıcal evıdence for effıcıent p-type dopıng of GaN usıng beryllıum, Appl Phys Lett Vol 70-22, (1997), pp 2990

[9] Dewsnıp *et al*, Photolumınescence of MBE grown wurzıte Be doped GaN, Semıcond Scı Technol , Vol 13, (1998), pp 500-504

[10] Sun *et al*, Actıvatıon of Beryllıum ımplanted GaN by two step annealıng, Nat Unıversıty of Sıngapore, (unpublıshed)

[11] Orton & Foxon, Group III nıtrıde semıconductors for short wavelength lıght-emıttıng devıces, Rep Prog Phys 61, (1998), pp 36

[12] Stotzler *et al*, Identıfıcatıon of Hg and Au defects ın GaN, Solıd State and Cluster Physıcs, Unıversıty of Konstanz (1998)

[13] Mah *et al*, Defect luminescence of GaN grown by pulsed laser deposition, Journal of Crystal Growth 222 (2001), pp 497-502

6 PLE System Development

6.1 Introduction

This chapter describes the development of a photoluminescence excitation (PLE) spectroscopy system The necessary steps taken and the components involved in implementing a PLE spectroscopic system are presented A PLE system consists of three main elements, namely, a tunable wavelength source, computer control / acquisition and collection optics Results based on this system are presented for ruby and GaN implanted with Be and Au impurities

6.2 Photoluminescence Excitation Theory

A photoluminescence excitation (PLE) system consists a wavelength tunable source exciting a sample where the exciting energy is varied from E_2 to E_1 (see figure 30) and the resulting luminescence is collected via a spectrometer fixed at a particular wavelength λ_0 [1] This isolates one luminescence band and provides information about the absorption energies required to excite that luminescence band [2] Whereas photoluminescence (PL) provides information about the ground states in the bandgap due to the crystal imperfections (impurities or intrinsic defects), PLE is able to access their excited

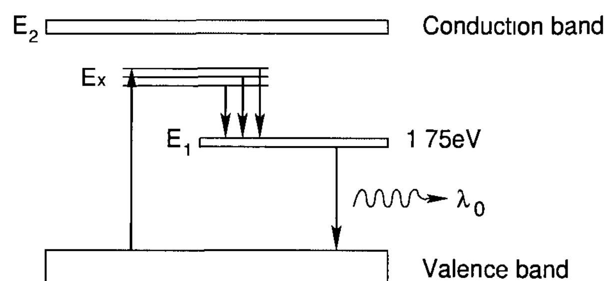

Figure 30 In a PLE system, excitation is in the region from the conduction band (E_2) to the energy level of interest (E_1) The presence of impurities and defects in a crystal can create energy levels within the forbidden band gap region (denoted by E_x) Electrons promoted to these defect levels can decay and feed directly into the level of interest, e g 1 75eV, where they can emit a photon of energy hv (λ_0)

states, which provides information about the absorption and emission of the electronic defects

6.3 Experimental System

This chapter outlines the development of a PLE system A description of the OPO laser is provided with the series of steps required to build an effective PLE system Figure 31 illustrates the PLE equipment arrangement which borrows much equipment from the existing PL system

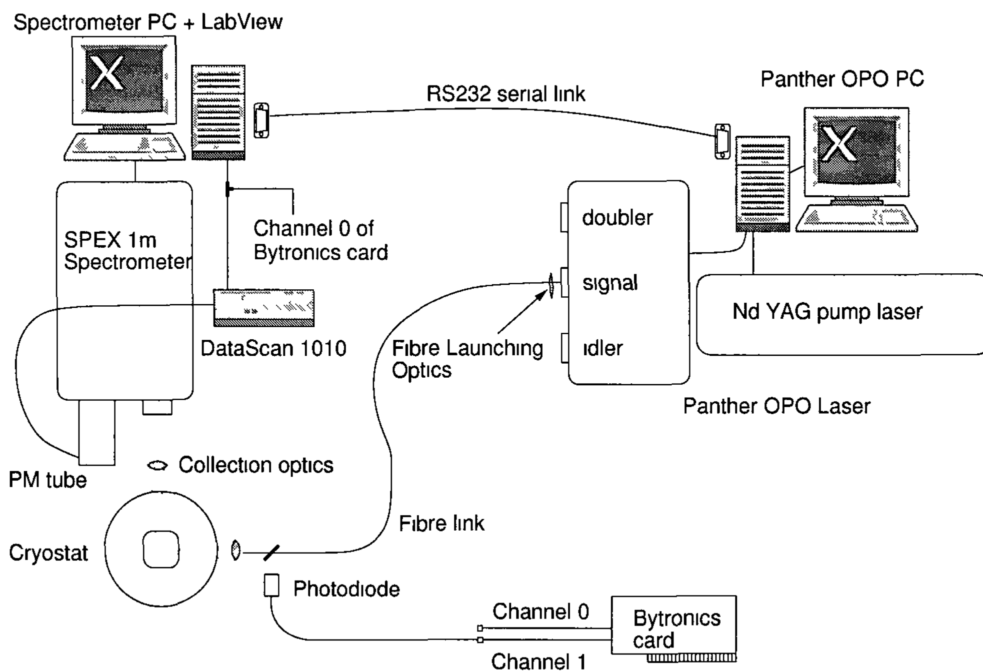

Figure 31 PLE setup showing, OPO tunable laser, computer control, signal acquisition and collection optics

6.3.1 OPO Excitation Source

In order to create a photoluminescence excitation spectroscopy system, a laser with a continuous variable energy range comparable to the energy range of excited levels of the defect under study is required The Panther OPO by Continuum lasers was chosen for this purpose

The Optical Parametric Oscillator (OPO) is a solid state tunable laser and a key component in photoluminescence excitation (PLE) spectroscopy The advantages of the (OPO) laser lie in its ability to quickly change wavelengths regardless of their separation The OPO (model Panther/Surelite II) supplied by Continuum lasers features tunable wavelengths from 0 2μm to 2 8μm

The OPO uses nonlinear materials in a laser-like cavity to generate two lower frequencies (i e longer wavelengths) from one input frequency [3] The shorter of these new wavelengths is called the signal wavelength, and the longer, the idler The exact values can be smoothly varied by tuning the cavity and rotating the OPO crystal under microprocessor control Because of the high power necessary for OPO operation, these devices have been limited to Q-switched and modelocked systems with a typical pulse repetition frequency of 10Hz The pump source for the OPO is a Nd YAG laser operating at $\sim$ 300mJ and $\sim$ 6ns pulse width (FWHM) at a pulse repetition rate of 10Hz (at 532nm) The optical parametric process is a three photon interaction in which one photon splits into a pair of less energetic photons The higher energy photon produced is referred to as the signal, while the lower energy photon is called the idler Because energy and momentum must be conserved, the system is constrained by the following [4]

$$E_{pump} = E_{signal} + E_{idler} \tag{10}$$

and

$$n_p/\lambda_p = n_s/\lambda_s + n_i/\lambda_i \tag{11}$$

The latter equation is referred to as the phase matching condition Because the index of refraction varies as a function of wavelength and the angle between the beam propagation and the crystal axis, only a single pair of

wavelengths, λ_s and λ_i, satisfy the above equation at a given angle for most crystals The wavelengths that do satisfy this equation vary smoothly with this angle Therefore, wavelengths from near-the-pump wavelengths to substantially longer ones can be generated simply by rotating the crystal The most common method to achieve the simultaneous conservation of energy and momentum takes advantage of the birefringent properties of a transparent nonlinear crystal such as BBO (β - barium borate) The signal output from

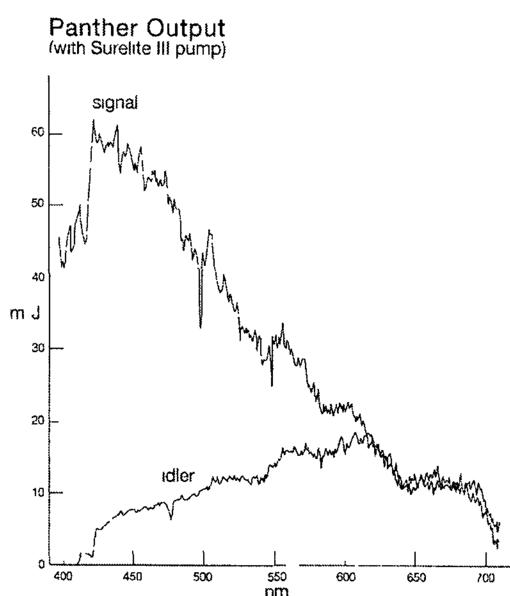

Figure 32 Power spectrum of OPO from 410nm to 710nm [5]

the OPO provides continuously variable wavelengths from 410nm to 710nm Figure 32 illustrates the signal and idler power outputs over this range The laser linewidth was measured as 0 24nm at 590nm In order to probe the bandgap energy of GaN, operation of the OPO is the region of 340nm was required This requires the doubling of the signal and is achieved through a change of internal optics This redirects the pump beam to a specific region of the OPO designed for doubling the signal and idler beams The output is in the form of a combined doubled idler and signal beam which are then spatially separated using a Pellin-Broca prism which maintains constant output beam direction

6.3.2 System Development

Referring to figure 31, it can be seen that due to physical constraints, the laser signal is transported to the cryostat windows using a 20 metre silica fibre (1000μm diameter with average transmission of 99% per metre over the range 300nm to 2000nm) This fibre has a quoted power handling capability of 25MW pulsed and 5kW continuous which was well within the requirements of this study

In order to remotely operate the OPO laser a 20 metre RS232 serial line was used to control the wavelength output Continuum lasers supply a series of commands designed for wavelength and laser control via the serial port (see figure 33) For the purposes of a PLE system, only a limited subset of these commands are required Programming the data acquisition, serial port and PLE display is done using LabView ^{TM} (National Instruments) [6] - a visual development environment Communication to the serial interface is performed using half duplex mode This reduces the complexity of interpreting returned scan status information The OPO is controlled in 'burst' step scan mode where commands are sent in a serial fashion over the RS232 line The RS232 protocol has an inherent delay of up to 100ms This is accounted for within the data acquisition software The PLE user interface (virtual instrument) is shown in figure 34 A flowchart outlining the program steps is shown, see figure 35 Appendix B details the PLE LabView virtual instrument source code

A Hamamatsu photomultiliplier (PM) tube is used to detect the resulting luminescence The PM tube output is recorded using an analog to digital

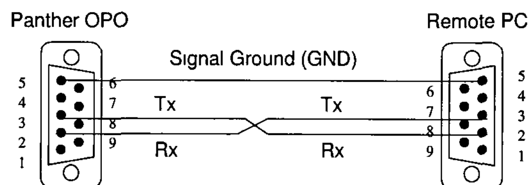

Figure 33 RS232 serial interface cable Connection are in a 'null modem' configuration with the transmit data (TX) and receive data (RX) lines crossed

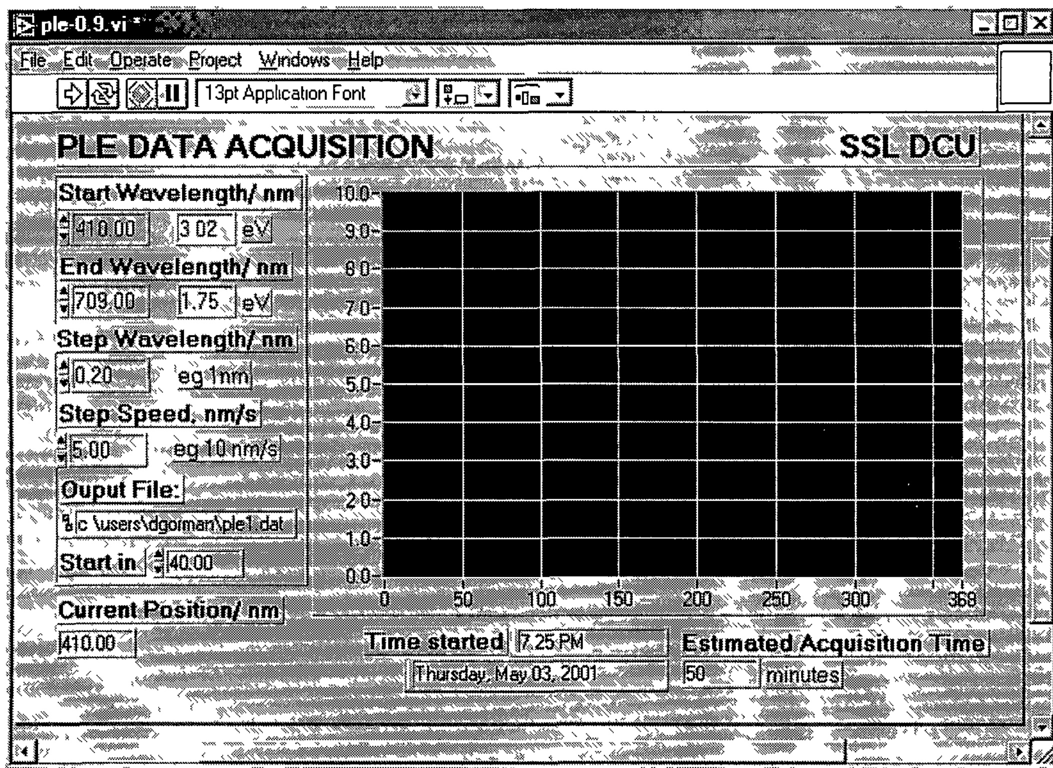

Figure 34 LabView GUI (Graphical User Interface) showing the virtual instrument front end for the PLE data acquisition system The user inputs acquisition parameters and luminescence data is plotted in real time on the chart Source code is given in appendix B

channel (ADC) on a Bytronics MPIBM3 interface card [7] Both this card and the LabView virtual instrument are set up to record data with 12 bit resolution Thus the detector output signal is sampled as a series of 4096 levels (2^{12}), a significant reduction in quantisation error over the alternative 8 bit (256 levels) conversion Using 12 bit resolution the time taken for recording and conversion is 25μs [7] While recording data it was found necessary to record and average the signal from the PM tube For each wavelength scanned, 10,000 points were recorded and averaged, taking a total time of approximately 250ms This method attempts to minimise the fluctuations in luminescence due to the pulsed nature of the OPO (10Hz) Another possible method suggested for future work would be to sample until

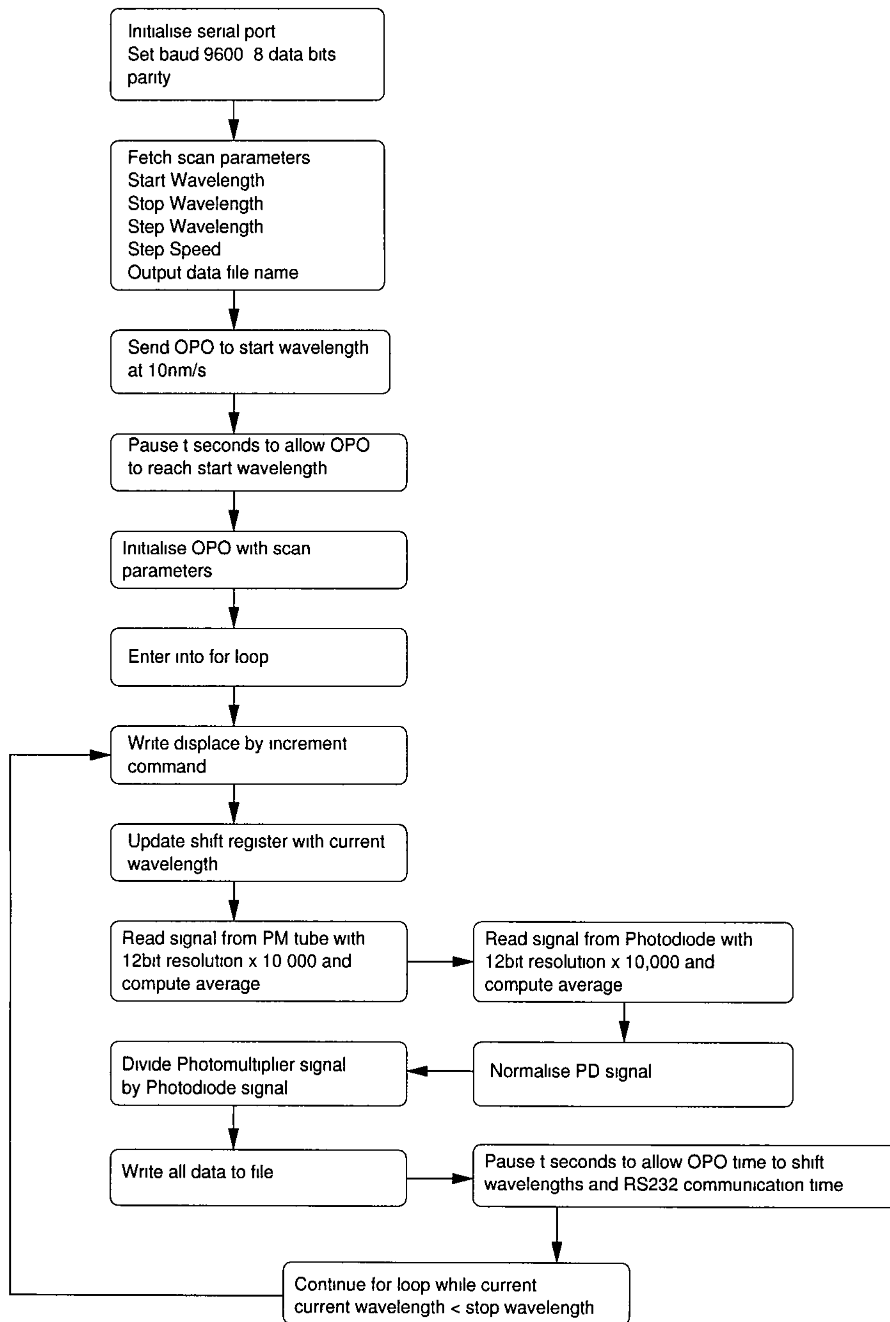

Figure 35 Flowchart outlining the LabView PLE data acquisition steps

a pulse is detected and record the resulting intensity This would require a timer circuit to sample and hold and then release at the appropriate moment

Another problem which required compensating for was that the output power of the OPO varies as a function of wavelength At each wavelength, signal normalisation [8] was achieved by sampling both the PM tube and the laser intensity meter and dividing both in software A laser intensity meter was fashioned by splitting a small amount of the laser signal ($\approx 4\%$) by reflection from a glass slide onto a Si PIN photodiode (Hamamatsu model S1223-01) and converting to a voltage using a 741 Op-Amp circuit [9] - see figure 36 The spectral response of the photodiode is reasonably linear over the required range (see figure 37) The output signal from this circuit is

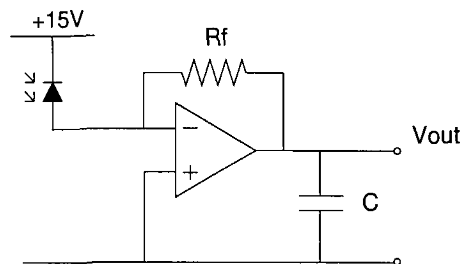

Figure 36 Photodiode in photoconductive mode used with a current to voltage converter $R_f = 6.8M\Omega$, $C = 0.047\mu F$

fed into an ADC channel on the Bytronics card and using 12 bit conversion the photodiode was sampled and averaged 10,000 times, again to account for the fluctuations in laser pulse energy It was seen using an oscilloscope that the decay time for each laser pulse emerging from the fibre is approximately 200ns and the time between pulses is 100ms The Nd YAG laser pumping the OPO has a quoted pulse duration of $\sim$ 6ns (FWHM) at a repetition rate of 10Hz It would appear that significant pulse broadening occurs in the OPO and the fibre The time window available for photodiode signal acquisition is 250ms or 2.5 times the pulse repetition rate Thus each 250ms window can contain a minimum of 2 pulses each with a decay time of 200ns, see figure 38(a) The result of this is an irregular sampling mechanism which either sampled on a peak occasionally or on a flat baseline When averaged 10,000

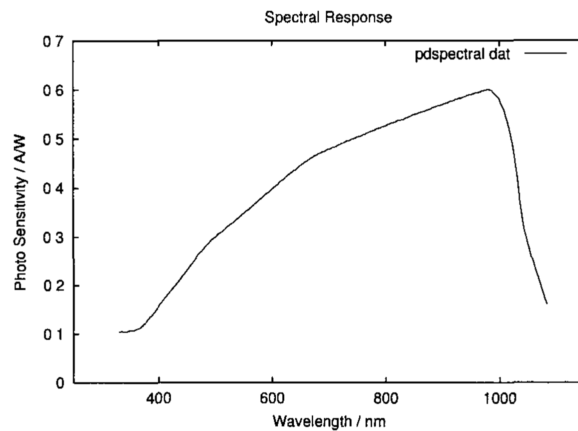

Figure 37 Silicon photodiode spectral response curve (Hamamatsu Si photodiode model S1223-01)

times the output was unacceptably 'noisy' - figure 39 shows an example of this Modifying the op-amp circuit reduced this problem (see figure 40) and

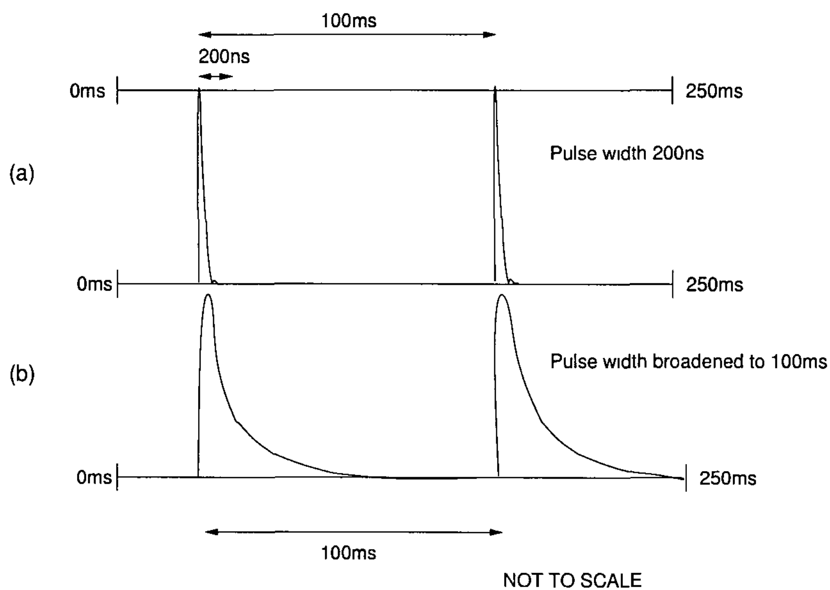

Figure 38 Laser pulses as detected by the intensity meter fashioned from a photodiode circuit Two pulses are depicted within the 250ms time window The original pulse width of 200ns is broadened to 100ms using a capacitor Samples are recorded every $25\mu s$ totalling 10,000 recorded points in the 250ms window

produced a more realistic curve in line with that achieved using a laser power meter This was achieved using a capacitor to broaden out the laser pulse length from 200ns to 100ms, see figure 38(b) 100ms is within the OPO pulse repetition rate and ensures an adequate sampling mechanism Figure 41 details the time allocated to each function for a single wavelength step

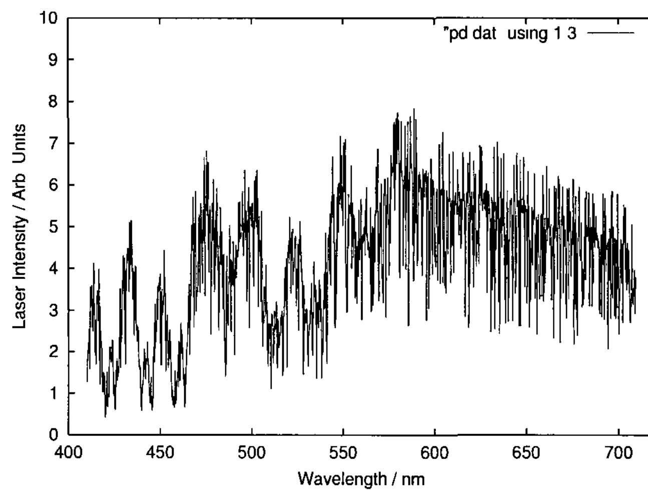

Figure 39 Laser intensity spectrum using a photodiode Spectrum is unacceptably 'noisy' as a result of poor sampling mechanisms

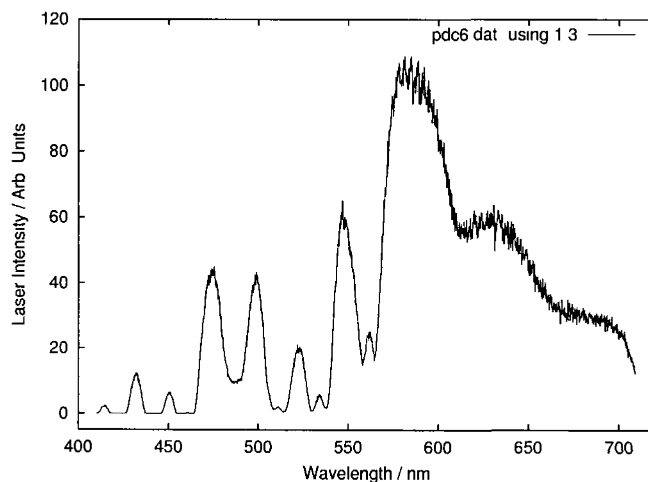

Figure 40 Laser intensity spectrum using photodiode but with a modified circuit

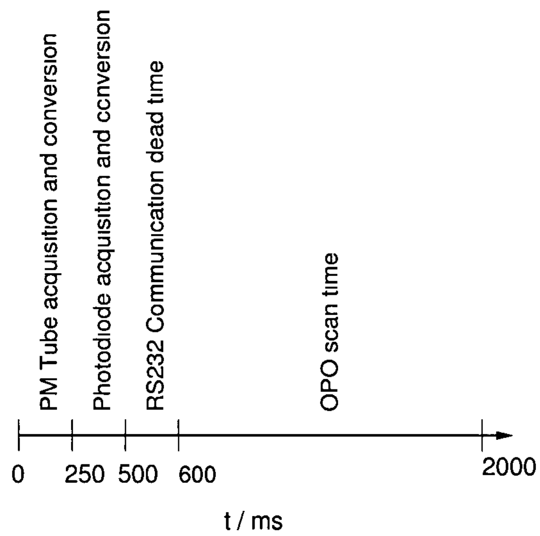

Figure 41 Timeline diagram outlining time taken for each acquisition and conversion step A buffer or 'comfort' window is built into the OPO scan time to allow for computer lag and minor variations in each of the estimated times

6.4 Conclusion

The work presented here represents a first step in testing the feasability of developing a PLE system using standard equipment and custom designed software As previously mentioned, minor problems remain in the PLE system due to the pulsed nature of the OPO laser These include the sampling mechanisms used for both the photomultiplier tube output and the laser power meter fashioned from a photodiode For future work, a sample and hold circuit is suggested where the samples are recorded until a peak is detected and the resulting intensity is fed to the data acquisition card

Also, the system needs to be integrated into the new SpectrAcq 2 system This requires the development of a frequency to voltage convertor for the output of the photomultplier tube to convert the pulses representing photons into a voltage level suitable for the Bytronics data acquisition card This will effectively bypass older data acquisition equipment

A method of smoothing out the fluctuations in the OPO power output as a function of wavelength would be highly desirable

References

[1] Perkowitz S , Optical Characterization of Semiconductors, (Academic Press London, 1993), pp 51

[2] Reuter *et al*, Photolummescence Excitation Spectroscopy of Carbon-doped Gallium Nitride, MRS Internet J Nitride Semicond 4S1, G3 67 (1999)

[3] Ambroseo J , Lasers Understanding the Basics, The Photonics Design and Applications Handbook, (Coherent Inc 2000), pp 195

[4] Radunsky M B , The OPO A Research Tool and More, The Photonics Design and Applications Handbook, (Continuum 2000), pp 243-246

[5] Continuum, Panther OPO Operation and Maintenance Manual, pp 4-4

[6] Labview Tutorial Guide, National Instruments

[7] Documentation for the Bytronic PC Interfaces Version 2 0

[8] McGlynn E & Henry M , Private communication

[9] Lawless B , Fundamental Analog Electronics, (Prentice Hall, 1996) pp 214-216

7 PLE Results

7.1 Introduction

An initial test of the PLE system was performed using a well characterised material, namely ruby Further studies are presented for Au and Be implanted GaN

7.2 Ruby Results

Test and development of the PLE system was performed using a ruby (Al_2O_3 Cr^{3+}) sample Ruby consists of Al_2O_3 doped with a small amount of chromium, the Cr^{3+} ions entering the host lattice substitutionally for aluminium ions A varying concentration of Cr^{3+} ions gives different levels of red colour to the material with a level of 1% being typical Figure 42 shows a room tempera-

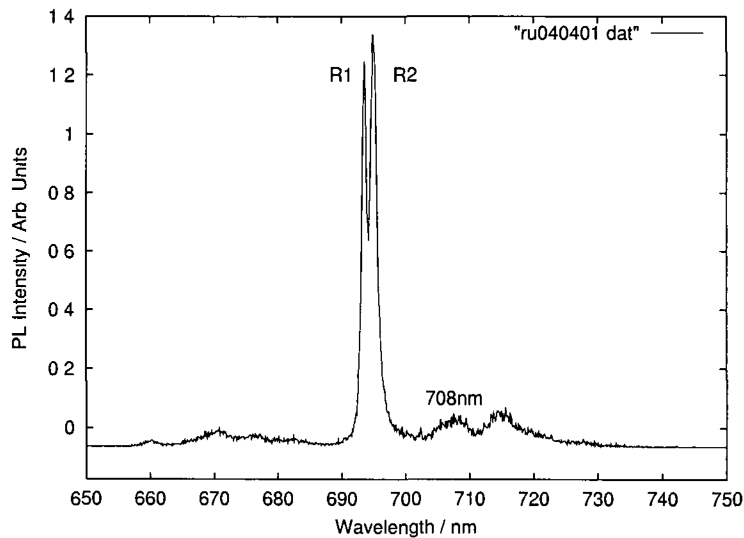

Figure 42 PL of ruby crystal From this spectra, the band at 708nm was selected for the purposes of acquiring PLE data

ture PL of ruby excited by the 442nm line of the OPO laser The absorption bands in ruby are broad and absorb in the blue and green spectral regions with narrow emission lines at 694 23nm and 695 67nm (referred to as R1

and R2 respectively [1] [2]) For the purposes of investigating the PLE system the feature at 708nm (1 75eV), referred to as λ_0, was selected The spectrometer is fixed at this band and the photomultiplier tube records the luminescence signal as the OPO scans through energies above this level The 708nm band was selected as it is the lowest available energy band within the PL spectra that matched the OPO's current wavelength range (410nm-710nm) Thus the luminescence band at 708nm is isolated and information is provided about the absorption energies required to excite this band The various energy levels feeding into this band are recorded and illustrated in a PLE spectrum, see figure 43 In this figure λ_0 can be seen to leak through at 708nm due to the laser light being scattered into the spectrometer as well as the distinctive R lines and associated phonon sidebands Figures 44 and 45

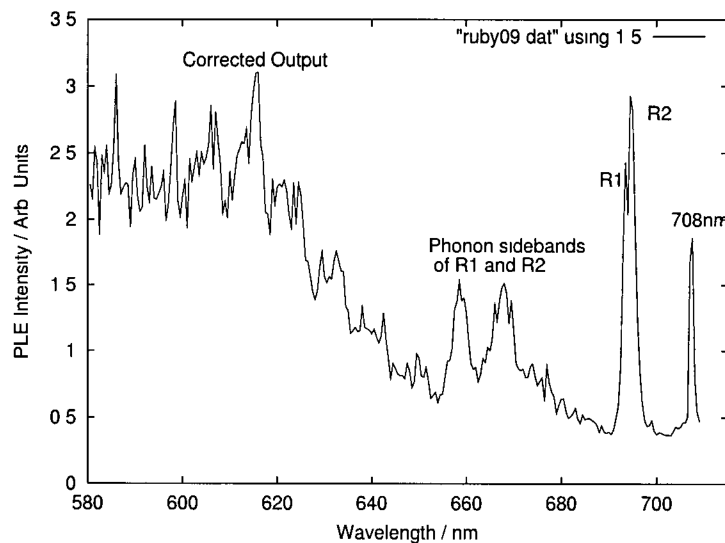

Figure 43 PLE of ruby crystal with $\lambda_0 = 708nm$ This spectrum is corrected for the laser power fluctuations but retains a large degree of noise R lines are clearly visible together with their associated phonon sidebands and laser leakage at λ_0

show the raw data obtained from both the photomultiplier tube and the photodiode respectively The data from the photomultiplier tube (figure 44) was normalised by dividing by the data from the photodiode (figure 45) It is noted that the photodiode signal appears quite noisy due to the fluctuations

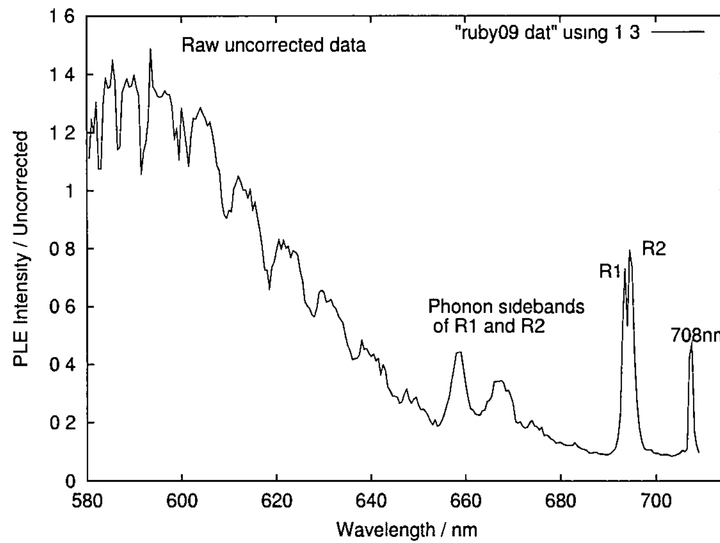

Figure 44 Uncorrected PLE showing the raw data from the photomultiplier tube prior to correction

in the OPO power output A much smoother and linear OPO power output as a function of wavelength would be highly desirable to minimise any deleterious effects upon normalisation

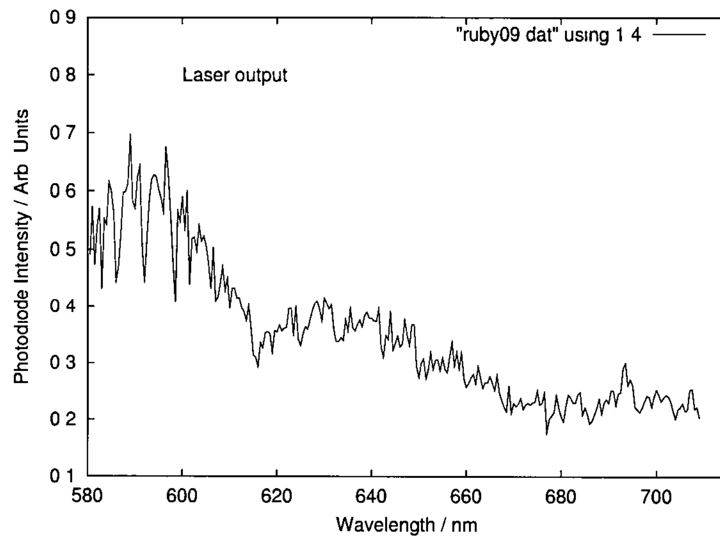

Figure 45 Photodiode intensity spectrum of the OPO laser The photomultiplier tube data is divided by this data to give the corrected output shown in figure 43

7.3 Au Implanted GaN

A PLE study of Au implanted GaN was performed at room temperature The strong yellow luminescence band at 550nm was selected for the purposes of this study with excitation in the bandgap region (see figure 46) To operate the OPO in this wavelength region a change of crystals is required The beam alignment and power were optimised to obtain tunable laser output in the region 355nm to 420nm

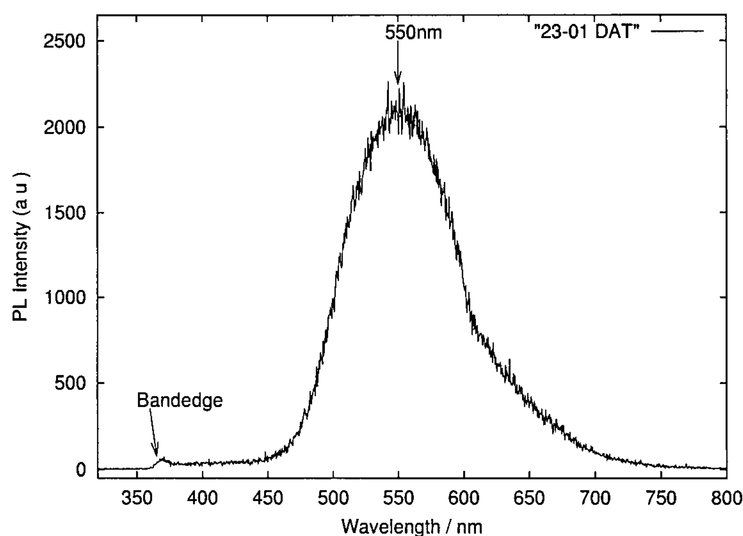

Figure 46 Room temperature PL spectrum of Au implanted GaN From this spectrum, the broad band at 550nm was selected for the purpose of acquiring PLE data with excitation in the region of the bandgap from 355nm to 420nm

Figures 48 and 49 show the raw data obtained from both the photomultiplier tube and the photodiode respectively Using the same method mentioned previously for ruby, the data from the photomultiplier tube (figure 48) was normalised by dividing by the data from the photodiode (figure 49) to produce the PLE spectrum shown in figure 47 Note that this corrected spectrum is quite noisy, however, a rough line is drawn through the noisy region at the bandgap ($> 3\ 3eV$) (see note 1) This noise, due to the variation in the OPO output power, presented itself as a particularly troublesome problem For example, investigating figure 47, weak peaks are seen at $< 3eV$, $> 3\ 1eV$

and > 3 2eV (see note 2) These correspond to mınıma ın the laser output power (see figure 49) The reason they appear as maxıma ın the corrected output (figure 47) ıs that the data ın figure 48 ıs dıvıded by the correspondıng small values ($\sim$ 0) ın figure 49 The detaıl referred to as note 3 ın figure 47 cannot be attrıbuted to any sıgnıficant feature due to the level of noıse resultıng from the laser power fluctuatıons

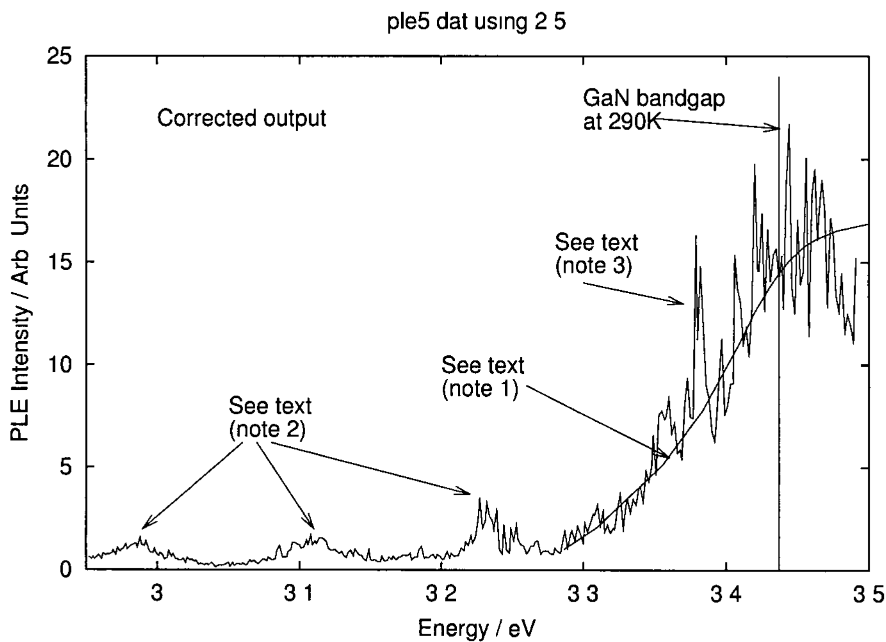

Fıgure 47 PLE of Au ımplanted GaN at room temperature performed wıth excıtatıon ın the bandgap regıon (from 355nm to 420nm) Thıs spectrum ıs corrected for the laser power fluctuatıons

Several tests were performed to determıne the effectıveness of the data acquısıtıon cırcuıtry Thıs ıncluded turnıng the power off to the photodıode cırcuıt and performıng a PLE scan ın order to check that both the photomultıplıer sıgnal and the laser power output was genuıne It was noted that a degree of crosstalk occured between the PM tube sıgnal and the photodıode cırcuıt Thıs has been attrıbuted to a capacıtıve effect on the Bytronıcs sıgnal ınput lınes due to theır close physıcal separatıon

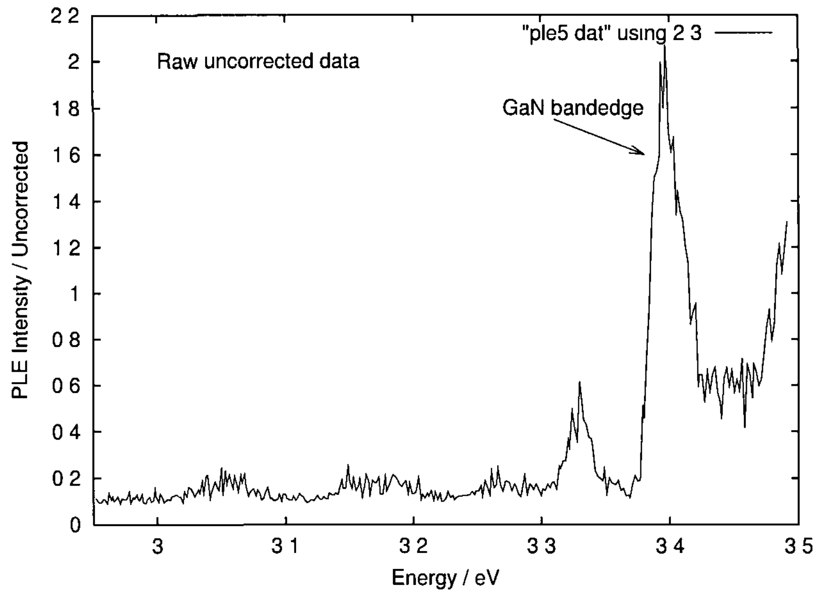

Figure 48 Uncorrected PLE showing the raw data from the photomultiplier tube prior to correction

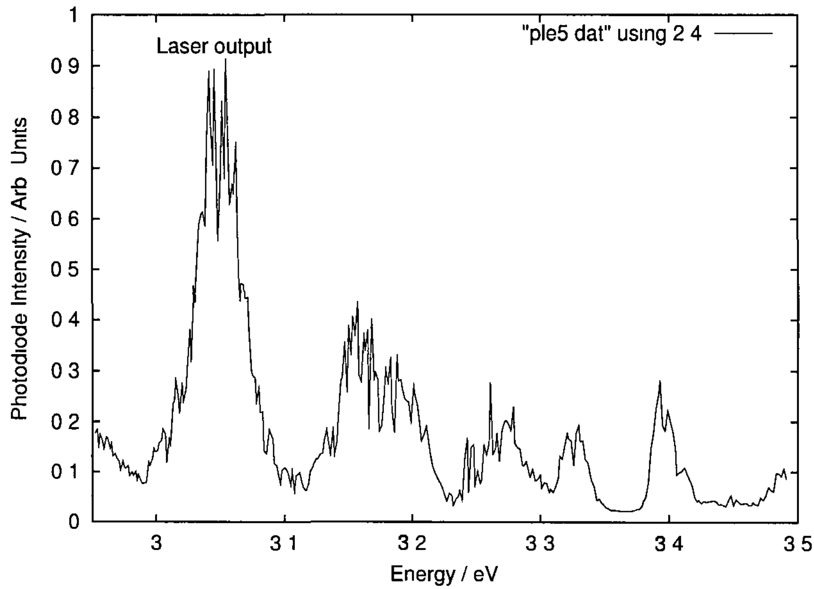

Figure 49 Photodiode intensity spectrum of the OPO laser The photomultiplier tube data is divided by this data to give the corrected output shown in figure 47

7.4 Be implanted GaN

A PLE study of Be implanted GaN at $1 \times 10^{12}\text{cm}^{-2}$ was performed at room temperature. The PL spectrum at 290K shows a yellow band at 550nm similar to that seen in Au implanted GaN. As for the previous case, this band was selected for the purposes of a PLE study with excitation in the bandgap region (from 355nm to 420nm). Figure 51 shows the PLE spectrum obtained at room temperature (corrected for laser power fluctuations). The raw, uncorrected, data from the photomultiplier tube and the photodiode are shown in figures 52 and 53.

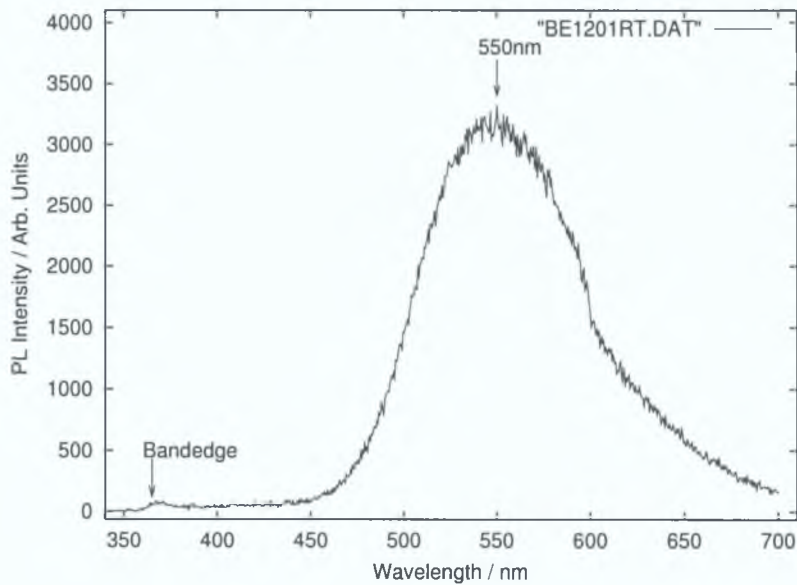

Figure 50: PL spectrum of Be implanted GaN at $1\times10^{12}\text{cm}^{-2}$ performed at 290K. From this spectra, the band at 550nm was selected for the purpose of acquiring PLE data.

Examining the PLE spectrum in figure 51, the line at 3.44eV represents the bandedge of GaN at room temperature. The corrected spectrum is quite noisy, however, a rough line is sketched through the noise at the bandgap region (see note 1). The band clearly visible at 3.35eV was seen as the dominant feature in previous PL studies (see figure 18) and is attributed to Be impurity centres. The local maxima at $< 3eV$, $> 3.1eV$ and $> 3.2eV$ (see

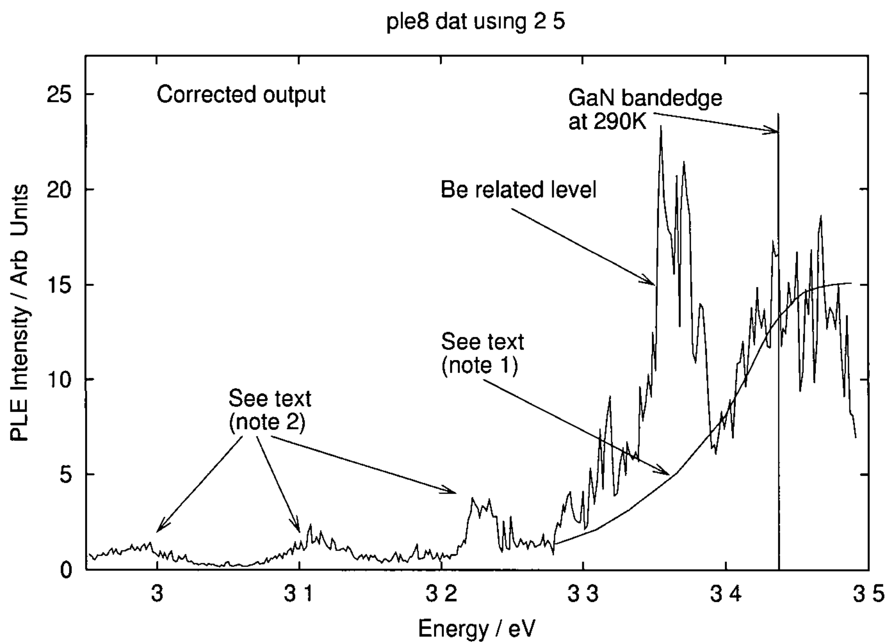

Figure 51 PLE of Be implanted GaN at $1 \times 10^{12} cm^{-2}$ with excitation performed in the bandgap region (from 355nm to 420nm) at 290K This spectrum is corrected for the laser power fluctuations

note 2) again arise for the same reason previously explained for Au implanted GaN

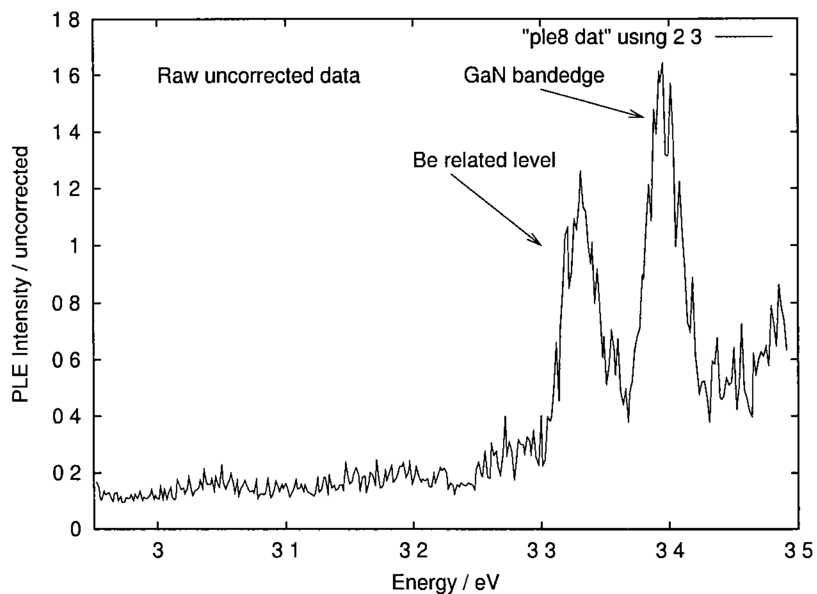

Figure 52 Uncorrected PLE showing the raw data from the photomultiplier tube prior to correction

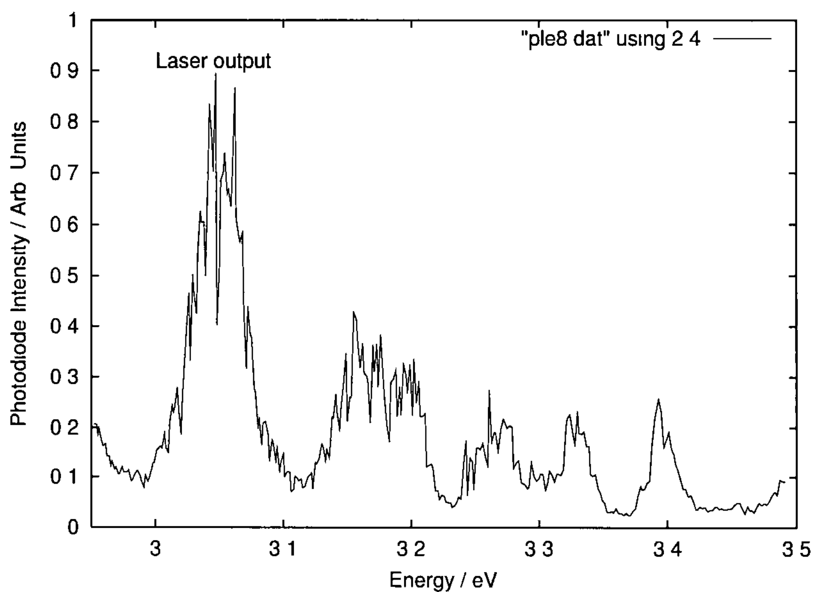

Figure 53 Photodiode intensity spectrum of the OPO laser The photomultiplier tube data is divided by this data to give the corrected output shown in figure 51

Figure 54 illustrates a combined PL and PLE spectrum of figure 18 (on page 36) and figure 51 Note that the PL spectrum was performed at 10K and the PLE spectrum at 290K The Be related feature at approximately 3 35eV in the PL spectrum roughly coincides with the Be feature in the PLE spectrum, with slight differences in energy attributed to the large temperature differences The PL spectrum was weak and showed no bandedge luminescence as was previously seen 15 months earlier in the same sample

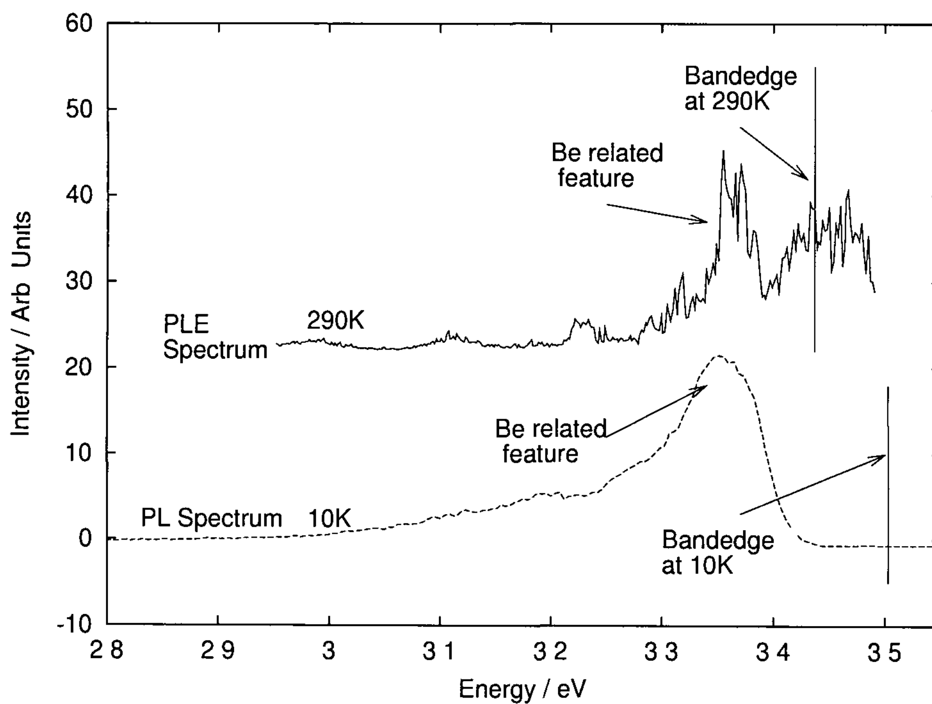

Figure 54 Combined PLE and PL spectrum of Be implanted GaN at $1\times10^{12}cm^{-2}$ Intensities are not to scale

7.5 Conclusions and suggestions for future work

The work presented here represents a test of the feasability of generating useful data from the PLE system using a well documented material, namely ruby, and subsequently Au and Be implanted GaN PLE on the ruby sample was successful with clearly visible features including the R lines and associated phonon sidebands and the laser leakage at λ_0

A PLE study on Au and implanted GaN was performed at room temperature in the bandgap region The resulting PLE spectra showed a broad band from below the bandgap to just above the bandgap This band contained a high level of 'noise' due to the large fluctuations in the laser power output as a function of wavelength This was a significant issue and combined with the limitations of the data acquisition methods (see previous chapter) remains to be improved upon Despite these issues an initial base has been provided for future development of the system

A PLE study of Be implanted GaN was performed at room temperature using the same λ_0 value and excitation range as for Au implanted GaN A similar broad band was seen at the bandedge, however, an additional band attributed to Be impurity levels is observed at an energy roughly corresponding to a PL band This provides further confirmation of the existance of a Be related defect level in GaN The problems associated with noisy spectra mentioned for Au implanted GaN were also relevant here

The issue of crosstalk between signal lines on the data acquisition card remains to be solved It is suggested that the signal lines carrying the data from the photodiode and the photomultiplier tube are physically separated to reside on channel 0 and 7 instead of channel 0 and 1 This will require a software modification Grounding the tracks between these lines on the veroboard may also help Also, proper shielding should be employed with a suggestion of using twisted pair on the all signal lines

References

[1] Reılly A , Excıtatıon transfer ın ruby M Sc , Dept of Physıcs, Unıversıty College Galway, Ireland, (1976), pp 7

[2] Wılson & Hawkes, Optoelectronıcs - An ıntroductıon, (Prentıce Hall 2nd Ed 1989) pp 185

A Grating Efficiency equations

Using polynomial regression the grating efficiency curve on page 24 can be approximated to a 4th order polynomial give by equation 12 Also the photomultiplier tube efficiency curve can be approximated by a 6th order polynomial given by equation 13

$$y = -59\ 649 + 0\ 5479x - 0\ 00181x^2 + 2\ 5857 \times 10^{-6}x^3 - 1\ 3598 \times 10^{-9}x^4 \quad (12)$$

$$\begin{aligned} y = &-1056\ 763 + 10\ 6889x - 0\ 0424x^2 + 8\ 6543 \times 10^{-5}x^3 \\ &- 9\ 6602 \times 10^{-8}x^4 + 5\ 621 \times 10^{-11}x^5 - 1\ 336 \times 10^{-14}x^6 \end{aligned} \quad (13)$$

B LabView Source Code for PLE System

The LabView source code for the PLE graphical user interface (virtual instrument) is shown overleaf A flowchart outlining the program steps is illustrated in figure 35 on page 55 along with a screen shot of the user interface on page 54

PLE-0 9 vi 08-05-01

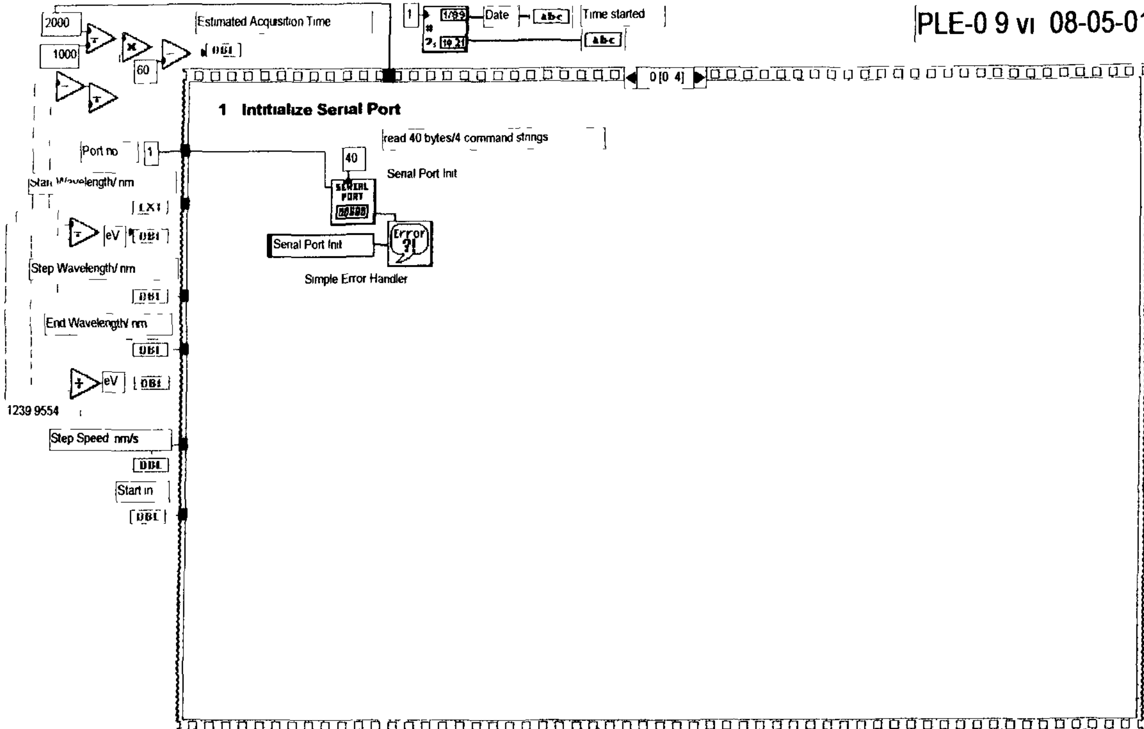

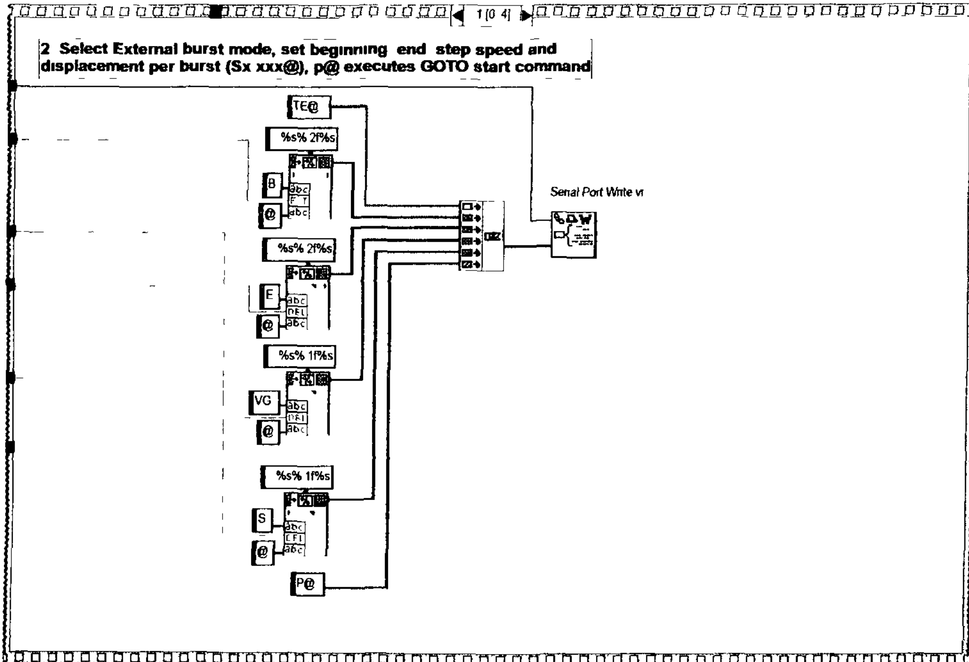

2 [0 4]

3 Pause for sufficient time to allow P@ command to reach the start wavelength

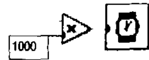

3 [0 4]

4.Enter into FOR loop read analogue input ports and collect data

Ouput File

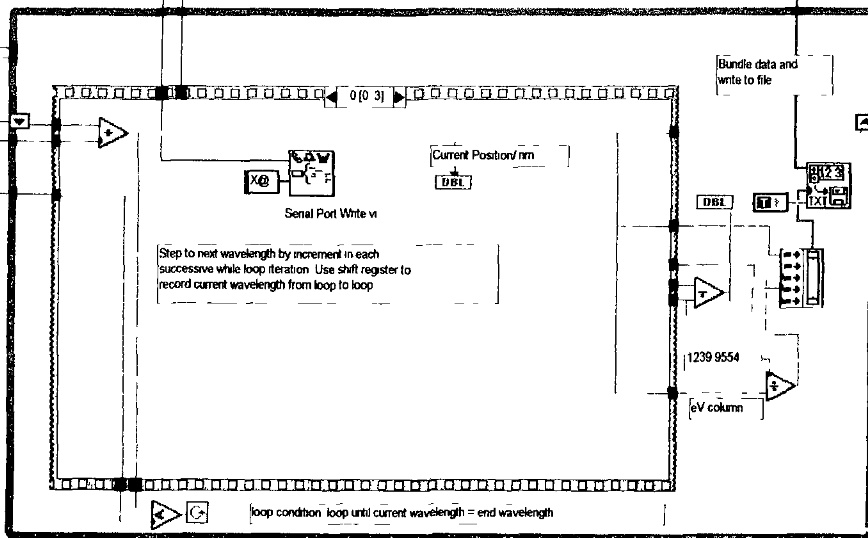

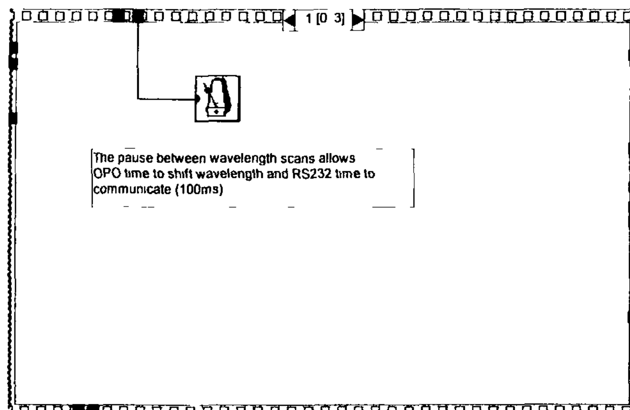
1 [0 3]
The pause between wavelength scans allows
OPO time to shift wavelength and RS232 time to
communicate (100ms)

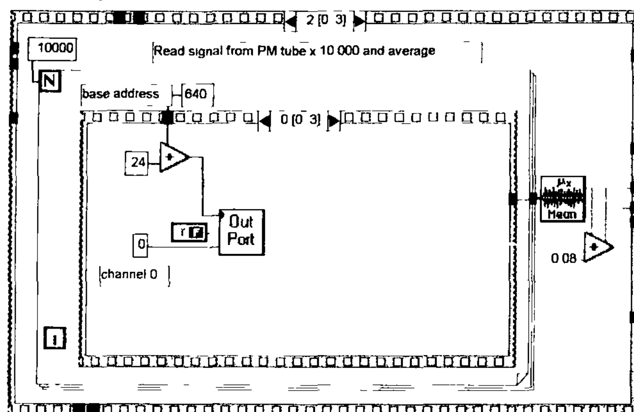
2 [0 3]
10000
N
Read signal from PM tube x 10 000 and average
base address
640
0 [0 3]
24
Out
Port
0
channel 0
Mean
0 08

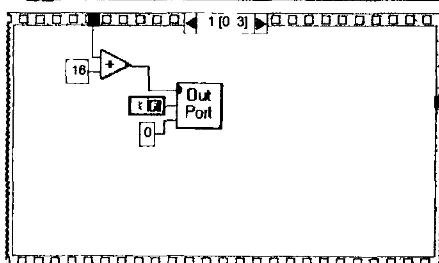
1 [0 3]
16
Out
Port
0

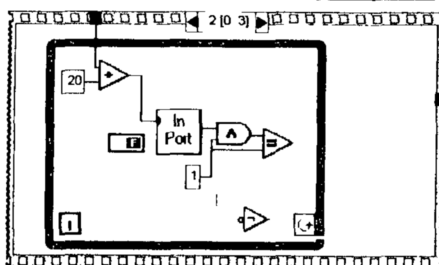
2 [0 3]
20
In
Port
1

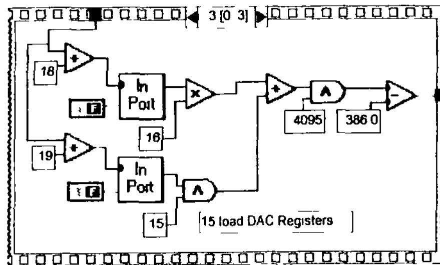
3 [0 3]
18
In Port
16
4095
386 0
19
15
15 load DAC Registers

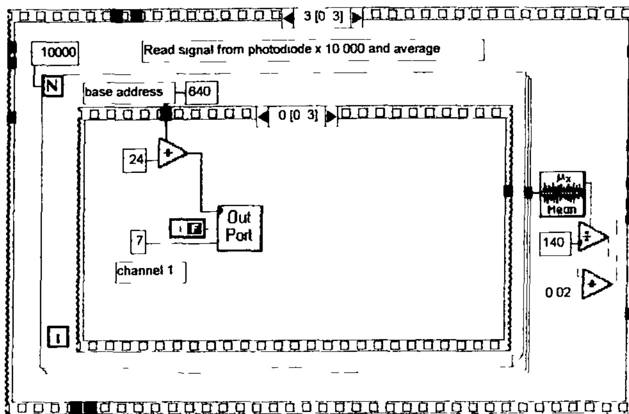
3 [0 3]
10000
Read signal from photodiode x 10 000 and average
N
base address
640
0 [0 3]
24
Out Port
7
channel 1
Mean
140
0 02

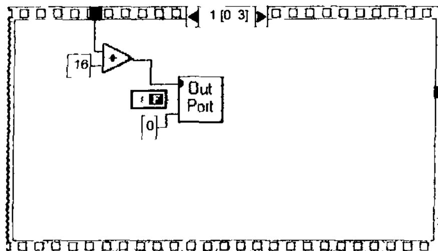
1 [0 3]
16
Out Port
0

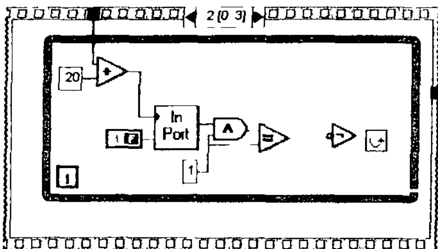
2 [0 3]
20
In Port
1

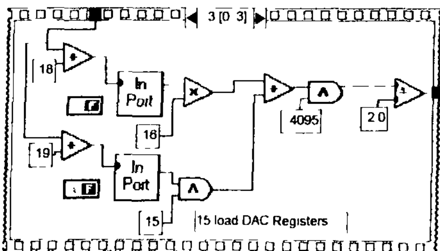
3 [0 3]
18
In Port
16
4095
2 0
19
15
15 load DAC Registers

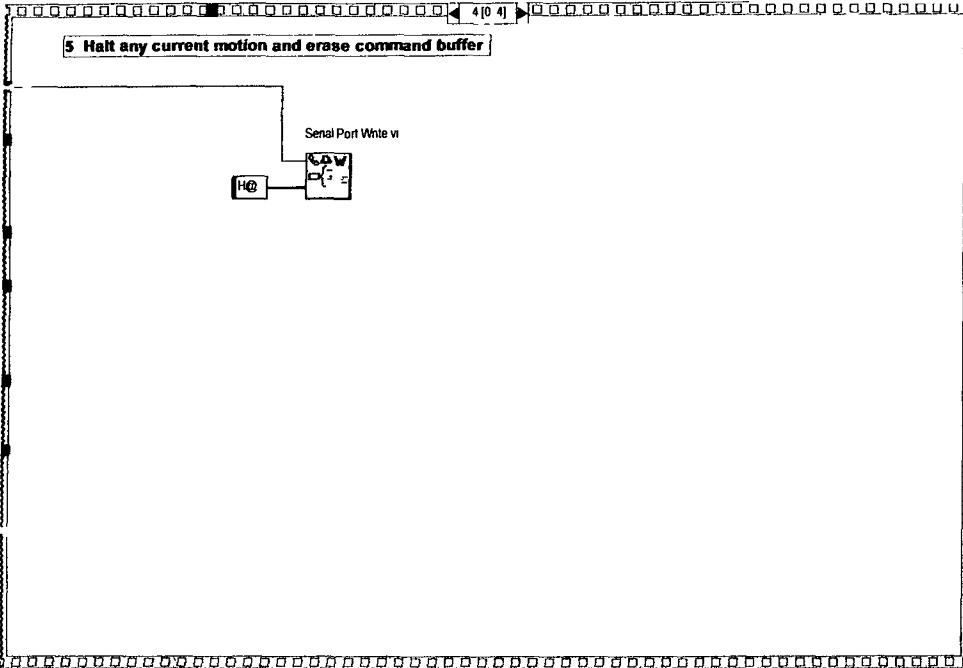

4 [0 4]
5 Halt any current motion and erase command buffer
Senal Port Wnte vi
H@

Typeset in LaTeX